Universidade de Aveiro
2012
Departamento de Engenharia de Materiais e Cerâmica

Pedro Tiago Albergaria Félix

Análise da bioactividade de cerâmicos ferroeléctricos seleccionados

Assessment of bioactivity of selected ferroelectric ceramics

Universidade de Aveiro
2011

PEDRO TIAGO ALBERGARIA FÉLIX

Análise da bioactividade de cerâmicos ferroeléctricos seleccionados

Assessment of biocompatibility of selected ferroelectric ceramics

Dissertação apresentada à Universidade de Aveiro para cumprimento dos requisitos necessários à obtenção do grau de Mestre em Materiais e Dispositivos Biomédicos, realizada sob a orientação científica da Doutora Paula Maria Lousada Silveirinha Vilarinho, Professora Associada no Departamento de Engenharia de Materiais e Cerâmica (DEMaC) da Universidade de Aveiro e co-orientação da Doutora Maria Helena Figueira Vaz Fernandes, Professora no Departamento de Engenharia de Materiais e Cerâmica da Universidade de Aveiro e diretora do Mestrado em Materiais e Dispositivos Biomédicos na Universidade de Aveiro, Portugal.

The Board of Examiners

President

Prof. Dr. Jorge Ribeiro Frade
Full Professor at University of Aveiro

Prof. Dr. Victor Miguel Carneiro de Sousa Ferreira
Associate professor at University of Aveiro

Prof. Dr. Paula Maria Lousada Silveirinha Vilarinho
Associate professor at University of Aveiro

Prof. Dr. Maria Helena Figueira Vaz Fernandes
Associate professor at University of Aveiro

agradecimentos

À Professora Paula Vilarinho por desde sempre ter sido uma inspiração, pelos conselhos e por todas as palavras de motivação.

À Professora Maria Helena Fernandes por me ter presenteado com a sua dedicação e conhecimentos e por ter sempre mantido o leme no sentido certo, mesmo quando o mar se apresentava agitado.

A todos os colegas dos Laboratórios do Departamento de Engenharia de Materiais e Cerâmica, nomeadamente ao Sebastian Zlotnik e Nathalie Barroca pelo apoio, dedicação e ensinamentos que me prestaram, assim como o suporte experimental e científico sem o qual o trabalho experimental não teria sido possível.

À Mariana Marinho e Micael Nascimento pelos ombros amigos, conselhos e presença nos momentos bons e menos bons.

À Sara Catita pela amizade e amor, pelas inúmeras vezes que me emprestou os seus ouvidos e por todo o apoio prestado, mesmo quando, por vezes, lhe era difícil.

Aos meus grandes e eternos amigos e companheiros de casa em Aveiro, nomeadamente ao Edgar, Simba, David, Márcio, Lucas, Joana, Luís, Martinha, Gustavo, Papa, Emanuel, Shakur, Pastor, Rui, Destrói, Marcelo, Carlos, Calças, Ivo, Lino, Mogli, Camilo, Bob, Bu, Chico, Lourenço, Diogo Mosca, Nobita, Nuno Coutinho, Tiago Marques e Santiago, por diariamente me fazerem chegar à conclusão que são aquilo que de mais precioso temos na Vida, por me apoiarem nos momentos difíceis e disfrutar da alegria nos nossos momentos mais “saborosos”.

Ao meu irmão, por sempre me ter apoiado, tomado o meu partido e dito as coisas que eu queria ouvir, nos momentos em que mais precisava ouvir.

Aos meus pais, pelo amor incondicional, pelo apoio e motivação que me foram dando ao longo de 24 anos.

palavras-chave

Correntes eléctricas endógenas, osso, bioactividade, cerâmicos ferroeléctricos, niobato de lítio, tantalato de lítio

resumo

Desde há muitas décadas que é sabido que os organismos vivos, em especial os tecidos, reagem fisicamente a estímulos eléctricos, podendo esses efeitos reproduzirem-se numa libertação de químicos endógenos, ou deformar a sua estrutura física. O tecido ósseo por si só é considerado um material/tecido piezoeléctrico, deformando-se mecanicamente quando lhe é induzido um estímulo eléctrico e vice-versa, ou seja, produz um potencial eléctrico quando sofre uma tracção ou compressão mecânica.

A hipótese de que um material ferroeléctrico possa vir a produzir efeitos no desempenho deste tipo de tecidos é então proposta, como por exemplo, para uma melhor, mais rápida e eficaz regeneração óssea. Estes mesmos materiais ferroeléctricos podem porventura alterar as cargas de superfície dos tecidos vivos de modo a atrair, atrasar ou até impedir o fluxo iónico de elementos químicos específicos responsáveis pelo processo de regeneração.

São escolhidos então o niobato de lítio e o tantalato de lítio como cerâmicos ferroeléctricos e foi estudada pela primeira vez a sua bioactividade *in vitro*, esperando-se encontrar pistas relativas à sua bioactividade *in vivo*. Estes cerâmicos ferroeléctricos foram seleccionados devido às suas importantes propriedades piezoeléctricas e ferroeléctricas. Estas propriedades podem abrir um novo e importante leque de aplicações biomédicas caso estes cerâmicos sejam bioactivos.

Este trabalho foi dividido em 3 fases: (i) sintetização dos pós de niobato de lítio e tantalato de lítio, (ii) caracterização dos pós e (iii) preparação das amostras e (iv) estudo da bioactividade destes cerâmicos ferroeléctricos.

Os pós foram produzidos através de um processo simples de mistura/moagem seguido de calcinação. Foram estudadas as fases cristalinas presentes através de Difracção de raios-X (DRX) e avaliadas as características morfológicas destes pós, nomeadamente o diâmetro de partículas e área superficial específica.

De modo a simular o ambiente do plasma humano, foi produzido sinteticamente um “Simulated Body Fluid” (SBF). Seguidamente as amostras foram imersas nesse ambiente líquido por 1, 3, 7, 15 e 21 dias. Após remoção dos pós foram realizadas uma série de análises de modo a estudar a sua bioactividade. De entre estes testes destacam-se a microscopia electrónica de varrimento (SEM/EDS), DRX e espectroscopia de Infravermelho por transformada de Fourier com reflectância total atenuada (FTIR-ATR).

Embora não tenham sido detectadas alterações no DRX realizado aos pós, verificou-se a formação de aglomerados de fosfato de cálcio na superfície dos pós através do SEM, resultados estes, reforçados pelo EDS e FTIR-ATR. Estes precipitados de fosfato de cálcio indiciam a capacidade destes pós cerâmicos ferroeléctricos se comportarem como bioactivos em contacto com tecidos ósseos *in vivo.*

keywords

Endogenous electrical currents, bone, bioactivity, ferroelectric ceramics, lithium niobate, lithium tantalate

abstract

For many decades it is known that living organisms, especially living tissues, physically react to electrical stimuli, and these effects may result in a release of endogenous chemicals, or deform its physical structure. The bone tissue itself is considered a piezoelectric material/tissue deforming mechanically when induced by an electrical stimulus and vice-versa, in other words, it produces an electric potential when it is submitted to a mechanical deformation.

The hypothesis that a ferroelectric material is likely to have an effect on the performance of this type of tissue is then proposed for, as an example, better, faster and more effective bone regeneration. These same ferroelectric materials may possibly change the surface of living tissues to attract, delay or even prevent the flow of specific ions responsible for the tissue regeneration process.

Lithium niobate and lithium tantalate were selected as ferroelectric ceramics and its bioactivity was studied in vitro and it is expected to find clues concerning its bioactivity in vivo. These ferroelectric ceramics were selected due to their important piezoelectric and ferroelectric properties. These properties may open up a new and important range of biomedical applications if they are proven to be viable bioactive ferroelectric ceramics. This work is divided into three phases: (i) synthesis of lithium niobate and lithium tantalate powders, (ii) characterization of powders and (iii) sample preparation and (iv) study of the bioactivity of these ferroelectric ceramics.

The powders were produced through a simple process of mixing/milling followed by calcination. Studies regarding the crystalline phases, particle size and specific surface area were made.

In order to simulate the environment of human plasma, a "Simulated Body Fluid" (SBF) was synthetically prepared. Thereafter, the samples were immersed in the liquid environment for 1, 3, 7, 15 and 21 days. After removal of the powders, a series of tests, namely SEM/EDS, XRD and FTIR-ATR were conducted to these powders in order to study its bioactivity. From these tests consisted mainly on SEM/EDS, XRD and FTIR-ATR. Although no changes were detected in the powders XRD, it was visualized by SEM the formation of agglomerates of calcium phosphate on the surface and these results were corroborated by EDS and FTIR-ATR. These precipitates of calcium phosphate suggest the ability of the ferroelectric ceramics to behave as bioactive in contact in bone tissue *in vivo*.

INDEX

Figure Index

Table Index

ABBREVIATIONS

DTA – Differential thermal analysis

EDS – Energy-dispersive X-ray spectroscopy

FTIR-ATR - Fourier transform infrared spectroscopy - Attenuated total reflectance

HAp – Hydroxyapatite

ICP – Inductively coupled plasma

JCPDS – Joint Committee on Powder Diffraction Standards

LNO – Lithium Niobate

LTO – Lithium Tantalate

PLZT – lead lanthanum zirconate titanate

PZT – Lead Zirconate Titanate

SBF – Similated Body Fluid

SEM – Scanning electron microscope

Tc – Curie temperature

TGA – Thermogravimetric Analysis

XRD - X-ray Diffraction

1. INTRODUCTION

1.1. Endogenous electrical currents in living organisms

The ability for humans and animals to generate endogenous electric signals, termed “animal electricity”, was documented in 1792 by Luigi Galvani when he noticed that an accidental sparked discharge caused frog muscle fibers to contract [1].

Figure 1 – Luigi Galvani (1792) [2]

Since this initial observation, it has been generally accepted that all organisms are electrodynamic systems, with large but stable gradients [3].

It has been reported that organisms from bacteria to mammals are sensitive to electromagnetic fields, [4] and these has been known to affect cell division rates, [5] tissue growth and wound repair [3]. So, through this knowledge it can be said that, tissues which generate endogenous electrical signals have a higher capacity to regenerate.

When a tissue has been damaged, injury potential creates steady electric fields, which exist locally for days after the insults. These potential differences result largely from ion flux through leaky cell membranes (Figure 2) and have been described as direct current-like, decay with time and have been estimated to be between 1 and 2 V/cm at the surface of wounds [6]. Wound healing is a dynamic response which occurrs together with cells, citokines, and enzymes, but research

has indicated that electrical gradients generated by injured tissue may be an integral part in the regeneration process [7].

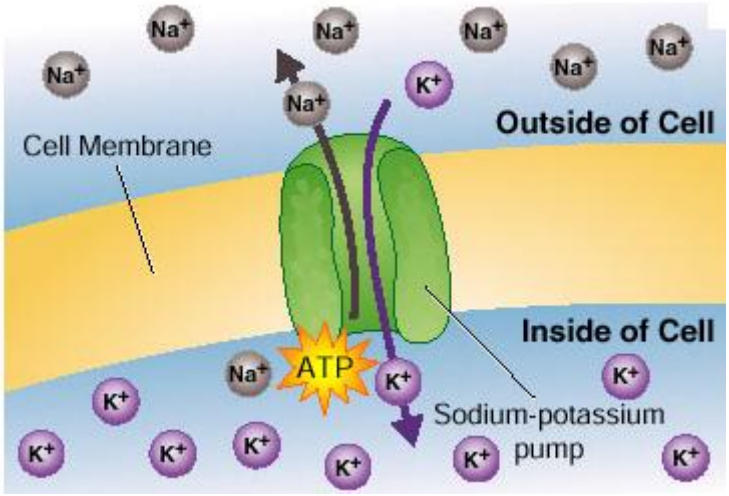

Figure 2 – Potential differences in a cell membrane; the ion exchanges are regulated by particular structures located within the membrane known as transport proteins. [8]

Measurements recorded during embryonic growth demonstrate that substantial endogenous current exist as early as fetal development [7]. These electrical signals function as a natural control system, ensuring proper cellular expression, [9] and facilitating cell migration and orientation, known as galvanotropism [6.10-12]. This ability cells are provided with also enable different immune responses, embryo development and the spread of cancer. All these governing electrical responses are present in all animals, but have been known to be uniquely dependent on species type. In the case of newts, who have the ability to fully regenerate injured extremities, large electrical currents have been recorded during the limb regeneration process (Figure 3) [8].

Figure 3 – Photograph of newt limb regeneration. Within 30 to 40 days, newts had regenerated their lost limbs and digits [13].

Observations that endogenous electrical currents affect tissue growth and repair has spurred interest in exogenous electrical stimulation from accelerating bone healing and remodeling in the field of orthopedics. However, exogenous electrical stimulation has been clouded with uncontrolled variations in experimental design [14] and the utility of these devices is still a controversial topic in the peer-reviewed literature [7,14]. Therefore, it is of scientific purpose to investigate the use of exogenous electrical stimulation for bone healing, to identify classical problems in order to improve the current understanding of this topic, and [5] to present evidence of future applications of electrical stimulation through the use of piezoelectric and ferroelectric materials.

1.2. Bone – from a transducer point of view

Bone is a highly organized, anisotropic tissue, [15] which serves as a reservoir for calcium and phosphate, a site for hematopoiesis and provides the structural support required for movement [16]. Bone remodeling is a dynamic system. [17] It is coordinated by cells, [18] hormones, [19] and enzymes, [17] and is strongly influenced by age, [20] activity level, [21] and mechanical loading. [22,23]

Physical forces exerted on bone alter bone architecture and is a well-established principle known as Wolff's Law [24].

It has been hypothesized by Frost [22] that a minimal effective strain is required to maintain bone architecture and physiology, and that bone strains rarely exceed 3% in vivo [26].

The principle that mechanical deformations of bone alter endogenous electrical signaling, and subsequent control of bone cell activity has been well regarded in the peer-reviewed literature [25,27]. However, it was not until the 1980's that the electromechanical properties of bone were postulated as a biophysical basis for Wolff's Law [27,28].

While it has been noted that mechanically deformed or actively remodeling bone always produces electrical current in vivo, [29] and is electronegative with respect to the resting environment, [30-33] bone formation and electrical stimulation were not initially considered to be an integrated system.

Successful bone growth results from a combination of both competent mechanical strain stimuli and endogenous electrical currents. [34] Correlations between bone formation rates and bioelectric potentials have been demonstrated by the ability of rabbit tibias to spontaneously generate potential differences up to mV in vivo [35].

The reformation that electrical signaling affected bone growth did not occur until stress generated potentials, known as piezoelectricity, emerged in the peer-reviewed literature.

1.3. The piezoelectric effect

Piezoelectricity was first reported by Jacques and Pierre Curie in 1880 when investigating the effect of charge generation through applied force in crystals of Rochelle salt (sodium potassium tartrate), quartz, and tourmaline. Piezoelectricity is characterized by a generation of electricity through applied pressure. This is known as the "direct piezoelectric effect", where a compressive or tensile force produces a potential difference across the opposite faces of the crystal. The "converse effect" is also observed such that a crystal will become strained in response to the applied electric field [36].

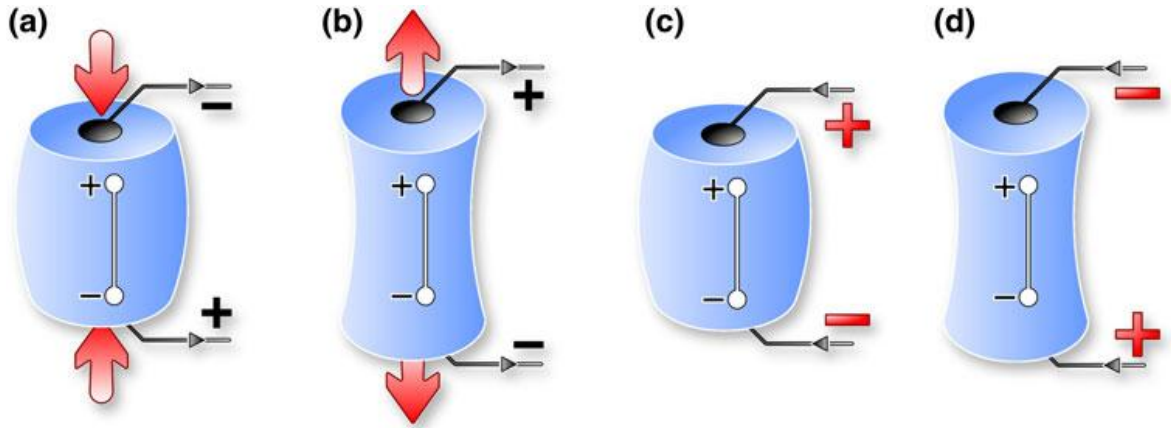

Figure 4 - Illustration of piezoelectric behavior. The direct effect: application of (a) compressive or (b) tensile force generates charge on the opposing faces and a potential difference. The converse effect: an applied electric field either (c) equal or (d) opposite of the material's polarity, causes the material to strain [37].

1.3.1. The piezoelectric effect – from an ionic flux point of view

Piezoelectricity can also be described by considering an ionically bonded crystalline solid and the distribution of ions within an individual unit cell. If this distribution of ions is asymmetric, an electrical dipole is generated [37].

When the dipole is mechanically strained, the movement of the positive and negative ions produce a net polarization – direct effect. On the other hand, the application of an electric field causes ionic movement, since alignment of the dipole with the field direction is preferable, producing a change in dimension of the dipole and a consequent mechanical change in the material at the macroscopic level – converse effect [36,37].

1.4. Piezoelectricity in the bone

The realization that biological tissue had the ability to generate electrical signals first was reported by Eiichi Fukada and Iwao Yasuda's work on piezoelectricity with mature rabbit's femurs in the 1950's [29,31,36-38].

Figure 5 - Eiichi Fukada - 1995 Recipient of the Jean-Leonard-Marie Poiseuille Award Outstanding and Creative Work in Electro-Biorheology and Hemorheology [39].

Bone specimens, harvested from human and ox femurs, demonstrated that stress-generated potentials were created by the shear forces of collagen fibers [38] and the deformation of fluid-filled channels, named Haversian and Volkman channels (Figure 6) [40,41].

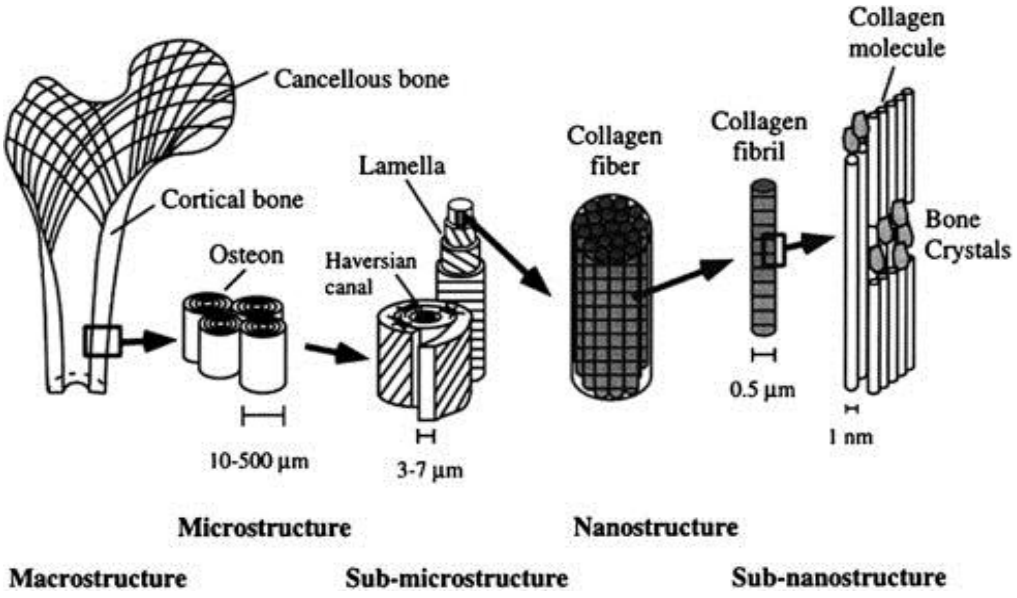

Figure 6 - Schematic of bone structure, demonstrating the position of the collagen fibers inside the Haversian canals [42].

Fukada and Yasuda noted that when a bone was submerged in acid for 3 weeks to remove the apatite crystals between the collagen fibers, electrical gradients were still produced [38].

Generation of electric potentials as described by Bassett and Becker [41] reaffirmed that mechanical deformation caused electrical stimuli and subsequently controlled osteogenic growth. Thus, the amplitude of electrical potentials was dependent on the rate and magnitude of bone loading, while polarity was determined by the direction of the deformed bone [44].

In vivo experimental recordings from the human tibia while walking has indicated a piezoelectric response as high as 300 mV [29].

The piezoelectric behavior of bone has been known to be strongly influenced by the state of the biological tissue. Because 10-15% of bone may be remodeling at any given moment, [18,45] there has been evidence to support natural variations in piezoelectricity over time [46].

Hydration of the host bone has been known to play an unique role in piezoelectricity, given that water distribution through the pores in bone and extracellular space naturally decrease over time and with progressive mineralization. [47] The piezoelectric coefficients decrease with increasing water content due to absorption of free water [47].

The clear coupling between mechanical forces and endogenous currents required for maintaining skeletal architecture has been clearly demonstrated since the 1950's. However, the use of exogenous electrical stimulation for expediting osseous growth dates back to the early 1840's [37,49].

In 1910 the Carnegie Foundation condemned the use of electrical stimulation and relegated electrotherapy to a scientifically unsupportable position causing it to fade almost completely from medical practice. [50]

Piezoelectric materials generally have some form of asymmetry, leading to the generation of an electrical dipole that reacts to an applied mechanical stress or an electric field. For the bone the electrical dipole seems to form as a result of asymmetric collagen molecules. Collagen fibers oriented parallel to the long axis of the bone which forms helices within the lamellae forming the Haversian systems, oriented at various angles [38,50,51].

The overall orientation of the collagen is generated in the direction of the bone axis and results in piezoelectric properties and the development of charge in response to the application of a mechanical load [36, 41-45, 51].

Figure 7 - The *annulus fibrosus* in human vertebrae with the *nucleus pulposus* removed. The collagen fibers are arranged in multiple concentric layers with consecutive rings running in alternating directions, left and then right, but always with an orientation of 65 degrees [52].

In addition to the piezoelectric effect, streaming potentials can also result in electrical activity in bone. The electromechanical properties of wet and dry bone are different and cannot be explained by a single mechanism: both streaming potentials and piezoelectricity are thought to occur in live bone [50]. The Extracellular Matrix (ECM) is negatively charged due to the presence of proteins. It is deformed in mechanical loading, inducing a flow of positively charged fluid and therefore developing streaming potentials [51,54].

The interstitial fluids (water solvent containing sugars, salts, fatty acids, amino acids, coenzymes, hormones, neurotransmitters, as well as waste products from the cells) are thought to move within bone canaliculi [54] which have a very small diameter in the order of 0.2 μm. Streaming potentials are thought to be part of the mechanosensory mechanisms in bone by which mechanical forces influence bone remodeling [50,53-55].

Within this context new generations of biomaterials are of interest in the current modern days; these materials seek to influence healing by mimicking the electrical effects in bone, namely the creation of a negative or positive charge on the surface of the biomaterial.

Two possible ways employed to create a surface charge are: [56]

- To polarize an ionic biomaterial by application of an electric field at elevated temperature to displace cations and anions in opposite directions.
- To develop a piezoelectric biomaterial so that a charge is generated under the application of a mechanical stress.

1.5. Ferroelectricity

Most of the investigations on piezoelectric materials have been carried out mainly on materials containing barium titanate or PZT [40,56].

Ferroelectrics represent a valuable subgroup of piezoelectric materials, characterized by the presence of a spontaneous polarization in the unstrained state and the capability to re-orientate in the orientation of polarization.

Ferroelectricity corresponds to certain crystal structures, of which the perovskite configuration is the most significant one, although it's not the only one existing for ferroelectric materials [56].

A better understanding of the ferroelectric phenomenon can be described by taking a look at small molecules. A molecule that is symmetric, such as methane (CH_4) has no dipole, but many simple molecules are not symmetric (e.g. H_2O) and have a dipole moment. It can be postulated that a structure that has a centre of symmetry cannot be ferroelectric. In other words, a ferroelectric material has a permanent electric dipole, and is named after and in analogy to a ferromagnetic material (e.g. Fe) that has a permanent magnetic dipole. Those that have a unique polar axis are ferroelectric and have a spontaneous electrical polarization. The others show the piezoelectric effect, wherein an electrical polarization is induced by application of an elastic stress; extension or compression will induce electrical polarization of opposite signs [57].

In terms of applied fields and polarization of the materials, when an electric field E is applied to an ideal insulator a short-range dislocation of the positive and negative charge centre causes the appearance of electric dipole moments in the material. The material is called a dielectric and is said to be polarized. If there is a linear relationship between the applied field E and the induced polarization P and P disappears when E is removed the material is called a linear dielectric [58]. This linear relation in the dielectric material is described in Figure 8.

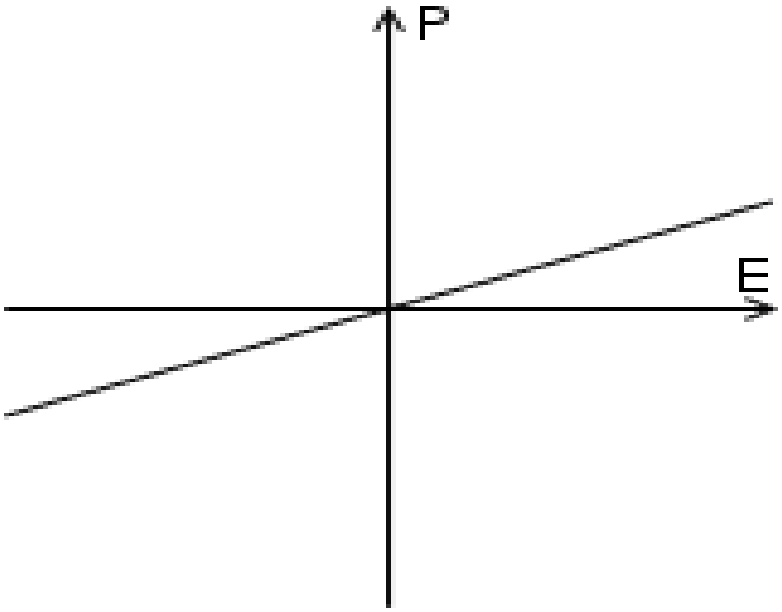

Figure 8 – Dielectric linear polarization [59].

If at zero field a mechanical stress provokes the development of electric charges (polarization) these materials are called piezoelectrics. Piezoelectricity is the ability of certain crystalline materials to develop an electrical charge proportional to a mechanical stress or vice versa [56].

In a piezoelectric the relationship between the applied deformation and the induced polarization is linear and reversible. In a piezoelectric the magnitude of P depends on the magnitude of the stress and the sign of the produced charge depends on the type of applied stress (tensile or compressive). If, in zero field conditions, there are dipolar moments due to a non-symmetric structure, the materials will have spontaneous polarization and they are called pyroelectrics. Some pyroelectric materials have an additional property; the direction of spontaneous polarization can be switched by an applied electric field. These materials are called ferroelectrics. All ferroelectrics are piezoelectric and pyroelectric [58].

In ferroelectrics the relationship between the applied field and the polarization is described by a hysteresis loop, which means that ferroelectric materials demonstrate spontaneous polarization at zero field and, as a distinguishing feature of ferroelectrics, the direction of the spontaneous polarization can be reversed by an applied electric field, yielding an hysteresis curve [56-58]. The electrical field at

which the polarization is reversed is called the coercive field (*Ec*) [58]. Figure 9 discribes a typical hysteresis loop of a ferroelectric.

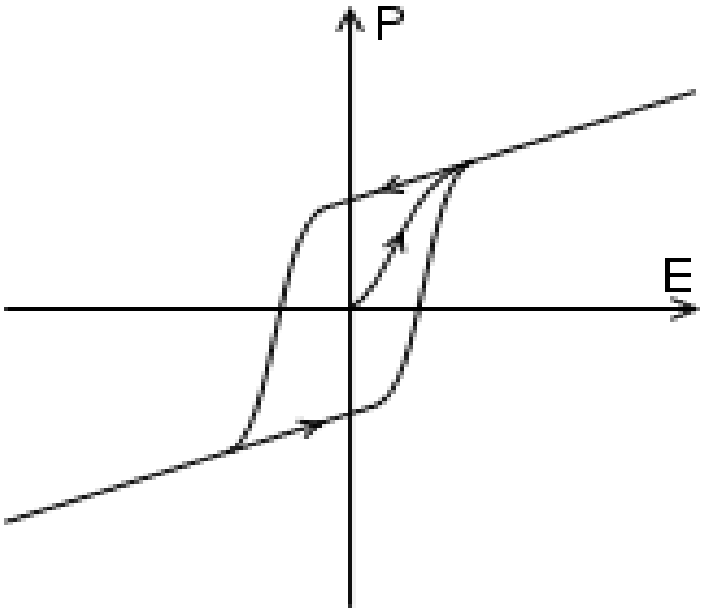

Figure 9 – Typical hysteresis loop of a ferroelectric, notice that the spontaneous polarization is present even at zero field after pooling [59].

Ferroelectricity is a phenomenon which was discovered in 1921 [56-61]. Ferroelectricity has also been called Seignette electricity, as Seignette or Rochelle Salt (RS) was the first material found to show ferroelectric properties such as a spontaneous polarization on cooling below the Curie point, ferroelectric domains and a ferroelectric hysteresis loop [60, 61].

A huge leap in the research on ferroelectric materials came in the 1950's, leading to the widespread use of barium titanate ($BaTiO_3$) based ceramics in capacitor applications and piezoelectric transducer devices. Since then, many other ferroelectric ceramics including lead titanate (PbTiO3), lead zirconate titanate ($(Pb[Zr_xTi_{1-x}]O_3$ $0 \leq x \leq 1$); PZT), lead lanthanum zirconate titanate ($(Pb_{0.83}La_{0.17}(Zr_{0.3}Ti_{0.7})_{0.9575}O_3)$; PLZT), and relaxor ferroelectrics like lead magnesium niobate ($((PbO)_3(MgO)(Nb_2O_5)$; PMN) have been developed and utilized for a variety of applications. Indeed, among inorganic crystalline ferroelectric materials, the perovksite group is particularly important, from the point of view of applications. These compounds have the general formula ABX_3, where

A is a large cation, B is a much smaller cation and X is an anion, usually oxygen (Figure 10). The B cation tends to be displaced away from the center and that is essential for the ferroelectric effect to exist [61].

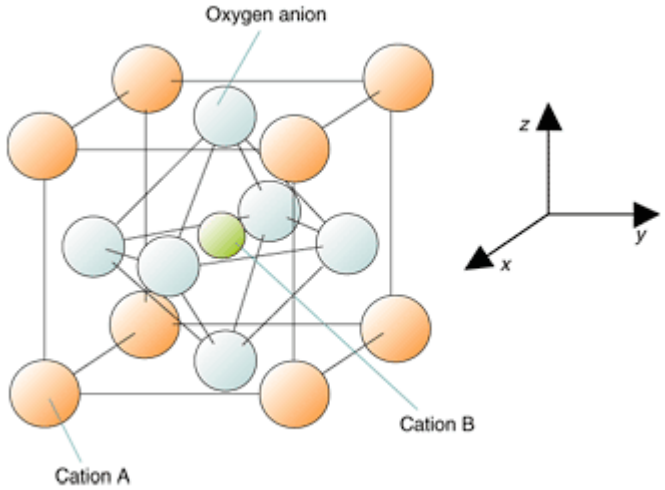

Figure 10 - Crystallographic structure of ABO_3 perovskite [62].

The materials with the highest piezoelectric coefficients belong to the lead based perovskite family. Besides the ability to design the physical properties required for certain applications, by formation of solid solutions, the possibility of fabrication as single crystals, ceramics, textured ceramics and thin and thick films adds value to this family of materials [58].

The biggest use of ferroelectric materials has been in the areas of dielectric ceramics for capacitor applications, ferroelectric thin films for non-volatile memories, piezoelectric materials for medical ultrasound imaging and actuators, and electro-optic materials for data storage and displays [60, 61].

As with the bone, the origin of piezoelectric behavior in ferroelectric materials comes from the formation of an electrical dipole due to an asymmetric distribution of ions [47, 58].

1.5.1. Ferroelectric ceramics as implant materials

If we take for example, $BaTiO_3$ as a ferroelectric ceramic, it is verified that at high temperatures, its structure has a simple cubic unit cell with large cations (Ba) at the corner sites, a smaller cation (Ti) in the body center and face centered oxygen ions (O) [60]. This symmetrical unit cell has no electric dipole and is neither ferroelectric nor piezoelectric.

Below a critical temperature known as the Curie point, *Tc*, the symmetrical cubic structure transforms to an asymmetrical structure, typically tetragonal or rhombohedral. Associated with this transformation is a spontaneous polarization, which results from the relative shift of ions with respect to the unit cell [36,56,57].

The displacement of the ions is restricted to specific crystal directions, allowing polarization toward one of the six faces in the tetragonal cell, or toward one of the eight corners for the rhombohedral phase [60].

Regions in a ferroelectric material such as $BaTiO_3$ where the unit cells have equal polarization directions are known as domains. After sintering a ferroelectric ceramic and cooling below the Curie temperature (*Tc*), domains will form in a random arrangement, such that there is no net polarization in the bulk material.

To align the domains in a single direction and make the material piezoelectric, it is necessary to “pole” the material [37,56].

1.5.2. Polling processes

The initial material consists of randomly orientated domains.

The material is heated to an elevated temperature below the *Tc* to facilitate domain motion, and a high electric field applied to orientate domains in a single direction [37, 61].

The domains move smoothly in response to the applied electric field [61].

The material is then cooled to room temperature while the electric field is still applied.

On removal of the electric field at ambient temperatures, the material retains a net polarization producing a poled ferroelectric ceramic with piezoelectric behavior, despite some domains may change direction [37].

1.6. Lithium Niobate and Lithium Tantalate as ferroelectric ceramics

Lithium niobate and lithium tantalate are two ferroelectric ceramics, which are important for applications in many technological fields [63, 64, 66].

They present ferroelectric properties at room temperature and may be grown in the form or large optical-quality single crystals [63,66].

In terms of crystallography, lithium tantalate and lithium niobate have similar crystallographic structures and consequently, same space group – R3*c*, with only slight differences in the lattice and positional parameters [64, 67-70].

Thus, the piezoelectric properties of LNO and LTO single crystals are highly dependent on the crystal orientation, which is related to the symmetry and the structure of these compounds. So it can be said, that in order to enhance the piezoelectric properties, the optimal directions of LNO and LTO should be considered [71].

In Table 1 there's a list of important properties and data relative to single crystals of lithium niobate, lithium tantalate and barium titanate.

Table 1 - Important properties of Lithium niobate, lithium tantalate and barium titanates [40,56-61,63,66,139].

	$LiNbO_3$	$LiTaO_3$	$BaTiO_3$
Stable Phase	Tetragonal	Tetragonal	Tetragonal
Molar Mass (g/mol)	233.192	147.846	235.887
Melting Temperature (°C)	1260	1650	1625
Density (g/cm^3)	4.65	7.45	6.02
Electrical Properties			
Curie Point (°C)	1210	610	135
Relative dielectric constant at 1 kHz (ε_{33})	27.9	42.8	109
Electromechanical Properties			
Electromechanical coupling factor (k_{33}) (%)	47	18	56
Piezoelectric charge coeficient (d_{33}) (10^{-12} C/N)	6	5.7/8	85.7
Piezoelectric strain coeficient (e_{33}) (C/m^2)	1.33	1.93	6.71

1.6.1. Lithium niobates main properties and applications

Ferroelectric properties in lithium niobate (M = 147.846) were first discovered by Matthias and Remeika in 1949. Lithium niobate is characterized by a trigonal crystal system and the respective space group is R3c. This material has a melting temperature of 1253ºC, which opened a wide window of applications as a ferroelectric and piezoelectric and may be utilized even more if proven bioactive and biocompatible [66].

Lithium niobate is an important functional material that has been widely used in the modern science and technology due to its large pyroelectric, piezoelectric, electro-optical, photo-elastic, ferroelectric coefficients and good optical, electric and electro-mechanical properties. With the development and application of functional devices, the synthesis of LNO powders attracts much attention and becomes an interesting topic in the field of LNO crystals, for instance, it can be utilized to create efficient holographic memory devices, second harmonic generation and optical parametric oscillation devices [72].

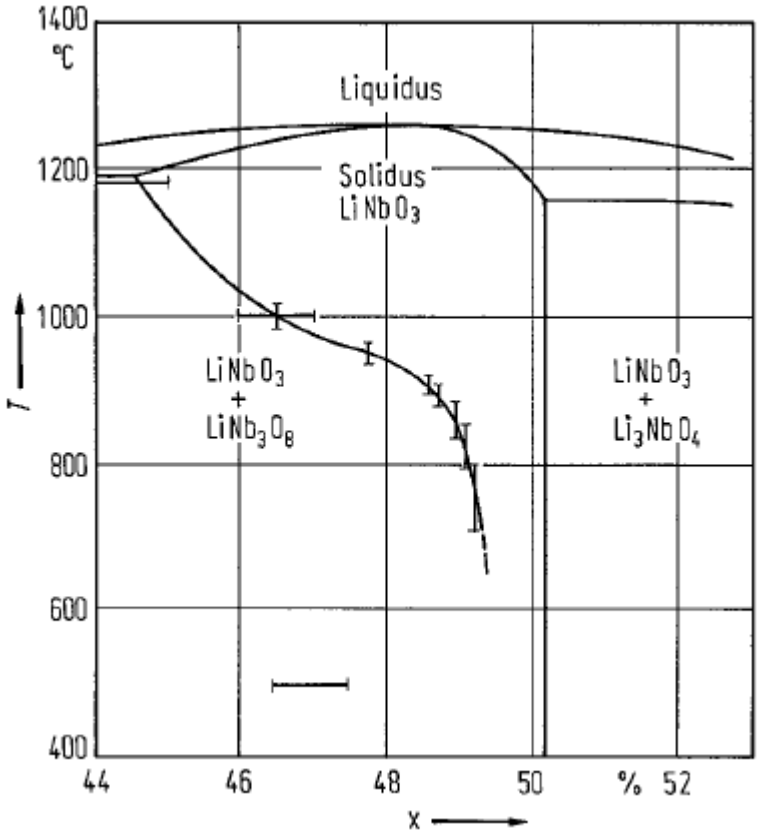

Figure 11 - LiNbO3. Phase diagram of system x Li2O·(1-x) Nb2O5 [73].

LNO powders were traditionally synthesized by the conventional high temperature solid-state method at 1200°C from the raw powders of Li_2CO_3 and Nb_2O_5, which often results in the growth of inhomogeneous large grains, the formation of additional phases (Nb_2O_5 and $LiNb_3O_8$) and possible loss of the crystal stoichiometry due to the easy volatilization of lithium at high temperature.

During the recent years, a number of wet chemical synthesis have been reported for the synthesis of LNO powders, such as the hydrothermal route [69], water-soluble complex method [72], solvothermal route [74] and metal alkoxides method [75].

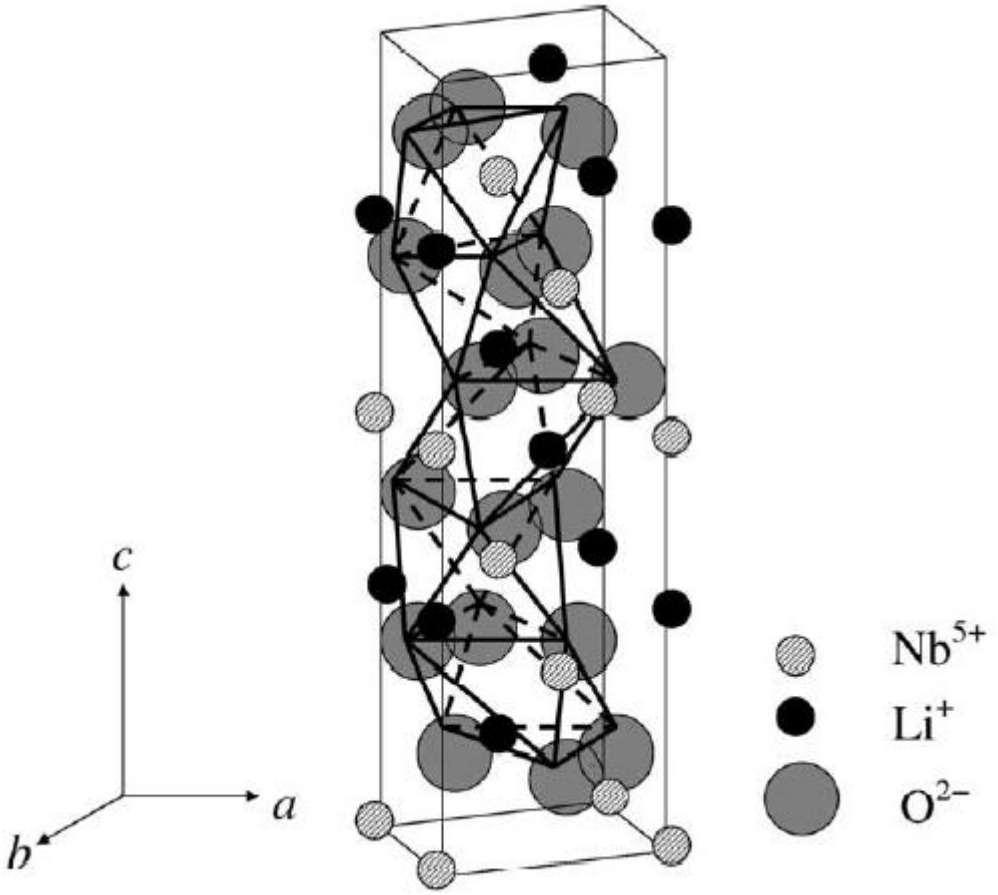

Figure 12 - Crystallographic structure of lithium niobate: view along the c-axis in one unit cell [76].

The crystallographic structure of LNO crystals consists of distorted oxygen octahedral by sharing their common faces along the c-axis lattice or edges at the ab plane, which forms a trigonal (c-axial) lattice. In the ferroelectric phase, both Nb^{5+} and Li^{+} cations are displaced from the centers of their respective octahedral [74, 75]. Additionally, in the three dimensional frame, NbO_6 octahedra link each other by sharing their common corners and the same happens for the LiO_6 octahedra [74-76].

1.6.2. Lithium niobate synthesis processes

The properties of ceramics are affected by the characteristics of the powder, such as particle size, morphology, purity, particle size, size distribution and chemical composition [63, 64].

The nature and quality of ceramic powders used in fabricating a final ceramic device or piece are key for determining the quality, yield and performance of that ceramic. This is especially true for the powders used in electronic ceramics [65].

1.6.2.1. Solid-state reaction

Solid-state reaction of lithium niobate is the traditional method for synthesizing powders, it is based on the simple mixing of the treated powder precursors through a mixing milling process, followed by calcination. The mixture is then re-milled if necessary (in order to remove agglomerates) and after shaping the green body is sintered at high temperatures [70-76].

Single-phase stoichiometric materials with a reproducible Li/Nb ratio are however difficult to obtain by solid-state reaction, due to the evaporation of Li_2O component at high temperatures. A reaction in the 1:1 mixture of Li_2CO_3 and Nb_2O_5 powders may yield Li_3NbO_4 and $LiNb_3O_8$ in the whole system, besides $LiNbO_3$ [71,73,74].

1.6.2.2. Chemical synthesis of stoichiometric lithium niobate powders

LNO powders may be chemically prepared by water-soluble complexes, this method is one of the reasonable ways to obtain stoichiometric lithium niobate powder [75].

The method involves milling Li_2CO_3 and Nb_2O_5 powders, followed by the addition of some urea powders. The misture is then put into a heater, the temperature of the heater is continuously increased and kept at 600ºC for 5h.

Despite the potential of such a water-soluble complex idea, there are still some problems existing in the wet chemical synthesis, such as the difficulty of solving niobium oxide and uneasy control of reaction conditions [77].

1.6.2.3. Combustion synthesis of Lithium niobate powders

The combustion synthesis is an attractive technique for producing LNO powders [75,77], whose advantages are that an organic compound like urea gives out heat that can be supplied to the precursors (Li_2CO_3 and Nb_2O_5 powders) in order to decrease the reaction time, and reduce the reaction temperature (600ºC). This method doesn't need any solvent involved in the reaction process (neither organic nor inorganic), thus the generation of impurities can be decreased [77].

The SEM micrographs in Figure 13 are here presented in order to further compare with the SEM results from the experiment presented in our own work.

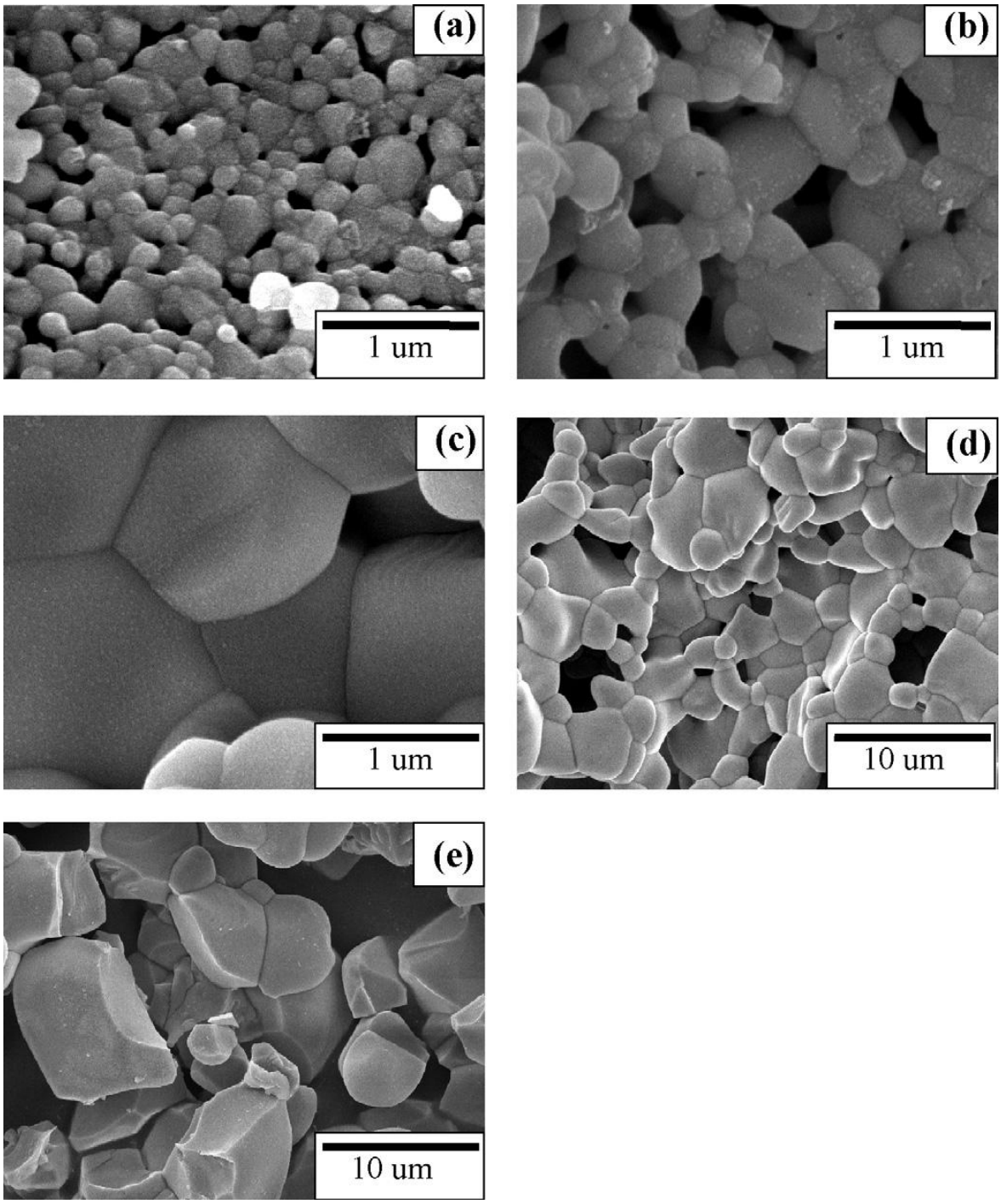

Figure 13 - SEM images of LNO powders produced by combustion method and calcined at various temperatures for 1 h. (a) 900°C, (b) 950°C, (c) 1000°C, (d) 1050°C, and (e) 1100°C [77].

1.6.3. Lithium Tantalate main properties and applications

Like with lithium niobate, ferroelectricity in lithium tantalate (M = 235.887) was first discovered by Matthias and Remeika in 1949, and this ferroelectric also has a stable trigonal crystal system and its space group is also R3*c*. Its melting temperature goes even further than that of lithium niobate which means its range of applications can be even greater (*Tmelt* = 1650°C). The crystallographic structure of lithium tantalate is very similar to lithium niobates [63-65,78,82,93-98].

Lithium tantalate is one of the most widely used electro-optic materials because of its excellent ferroelectric, piezoelectric, pyroelectric and photo-refractive properties [79-85]. It is also utilized in mobile telephones for intermodulation of saw filters, in infra-red image detectors, waveguide lasers and as acoustic wave devices to monitor enzyme concentrations [78-81,86-88]. It was also investigated as a photocatalyst for the reaction of photocatalytic hydrogen generation [88]. Although single crystals of $LiTaO_3$ have many applications, there are still some restrictions to its acquisition due to its high cost and difficult fabrication. On the other hand, polycrystalline LTO ceramics can be made with a larger size and more complex shapes [80]. Still, most studies were concentrated on the growth and properties of $LiTaO_3$ single crystal [79,83].

$LiTaO_3$ traditional powder preparation is based on the solid-state reaction, but this method requires heat treatment at relatively high temperatures (>1000 ^{0}C) and volatilization of Li_2O may occur [63-66,78-83,88-99]. This volatilization of Li_2O may happen due to its significant low vapor pressure at the processing conditions, which makes it difficult to control the stoichiometry [82-86]. Therefore, inhomogeneity in composition and coarse particles may be encountered. [78,84]

Various methods are reported in the peer-review for $LiTaO_3$ powder synthesis including sol-gel process, solid solution systems [79,85-88,92] and combustion, co-precipitation, hydrothermal, alkoxide and citrate gel methods. [57,63,65,78,80] Among these methods, alkoxides, hydrothermal and colloid emulsions are time consuming and involve highly unstable alkoxides, this causes difficulty in controlling and maintaining the reaction conditions [84].

1.6.4. Lithium tantalate synthesis processes

1.6.4.1. Solid-state reaction

Alike solid-state reaction of LNO powders, this solid-state reaction is the traditional method for sintering LTO powders. Solid state reaction although easy, may lead to composition inhomogeneity and coarse particles [100].

Thus, LTO is difficult to be sintered because of volatilization of Li_2O at high temperature (>1300 ºC) [65].

1.6.4.2. Chemical preparation of lithium tantalate powder

Chemical routes, such as precipitation from solution, or sol-gel processes, have received considerable attention [100]. These chemical routes can offer many advantages over conventional processes, such as high purity, and molecular homogeneity. These methods have been widely used for the synthesis of powders for electronic ceramics applications, such $BaTiO_3$ [102] and PLZT [104].

Jean *et. al.* [65], came up with a chemical preparation of spherical lithium tantalate powder method, by spray drying lithium tantalate percursors – lithium acetate and tantalum ethoxide. Hydrous lithium acetate was first dissolved into methoxyethanol and dehydrated at 125 ^{0}C for 30 min and precipitated anhydrous lithium acetate.

After cooling the acetate precipitate was redissolved at 125 ^{0}C and this cycling process continued for 2h to complete the chemical reaction between lithium acetate and tantalum ethoxide. The solution was cooled at room temperature and then spray dried [65].

Figure 14 will be useful for comparing this experiment with lithium tantalate in the results chapter.

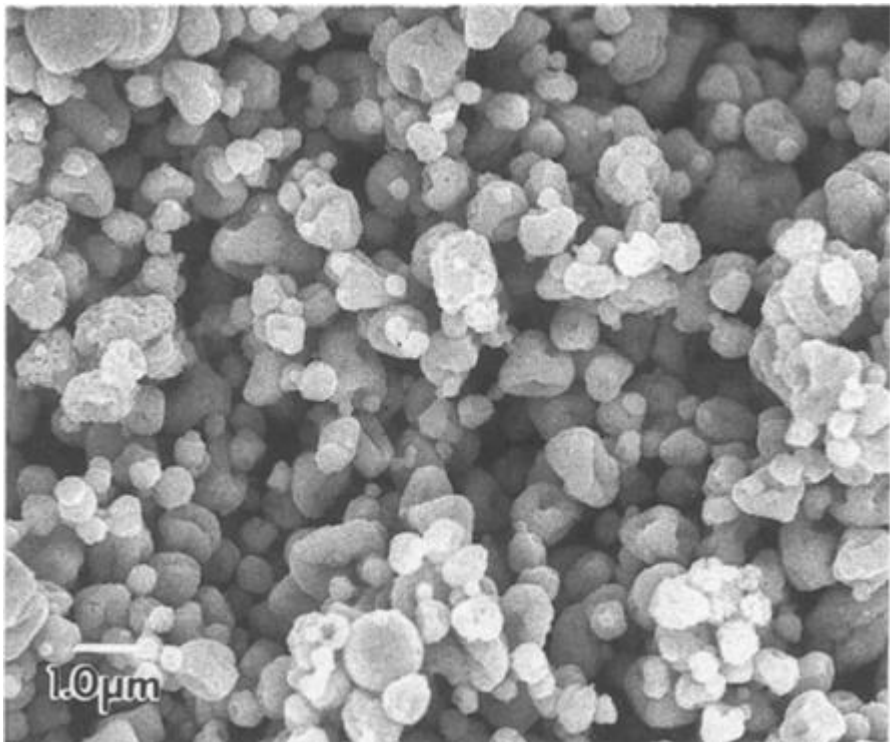

Figure 14 - SEM micrograph of lithium tantalate powder calcined at 800~ in air for 2 h prepared by jean et al. with a chemical route [65]

1.6.4.3. Combined hydrothermal and wet-chemical technique for LTO powder synthesis

Ta_2O_5 is very stable and can hardly be dissolved by regular wet-chemical routes. A successful attempt on dissolving tantalum (V) oxide was done by Muthurajan *et. al*, using hydrofluoric (HF) acid (40%) in a hot water bath for 10h. However, HF acid is strongly corrosive and toxic. It still remains a relatively difficult task to synthesize high quality LTO powders from nontoxic starting materials [101].

Zheng F. *et al.* [102], utilized a combined hydrothermal and wet-chemical technique to produce LTO powders, this synthesis method involves nontoxic raw materials, mainly tantalum hydroxide ($Ta(OH)_5$) and lithium carbonate ($LiCO_3$). $Ta(OH)_5$ was first dissolved in hydrochloric acid through a hydrothermal process, followed by addition of citric acid (CA) to form stable Ta-CA complex. After pH adjustment with ammonia and addition of Li_2CO_3, pure LT powders were obtained by calcination at 720 ^{0}C for 2h.

Compositional, microstructural, and morphological aspects of the final product were evaluated with XRD and SEM. Thermal behavior and calcination temperature were determined by thermal analysis [102]. In figure 15, there's a micrograph of LTO powders resulted from this experiment, the morphology of these powders is useful for future comparison.

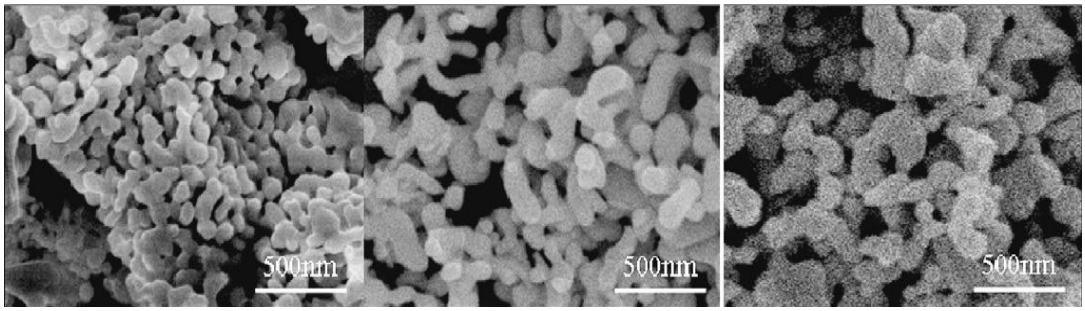

Figure 15 - SEM images of the LTO powders synthesized by a combined hydrothermal and wet-chemical technique at: (a) 570ºC, (b) 750ºC, and (c) 850ºC [102].

1.7. Bioceramics

Ceramic materials used to regenerate and replace damaged parts of the human body, are designated as bioceramics [103-112].

To be applied as biomaterials, these ceramics must satisfy certain biological conditions such as, non-toxicity, non-carcinogenic, not allergic, not inflammatory, biocompatible and biofunctional during the implantation period [108]. Bioceramics can be monocrystalline, polycrystalline, glass, glass-ceramic or composite.

The clinical success of a bioceramic depends, essentially, on the formation of a stable interface with the bone tissue and the combination of the mechanical properties of both implant and living tissue. The adhesion mechanism to the living tissue is directly related to the type of biological response induced by the bioceramic in the interface between the material and for example, the bone tissue [110-112].

There are four main kinds of biological response and adhesion processes that allow the distinguishing of bioceramics from one another, mainly, bioinert,

resorbable, porous and bioactive [112]. These four biological responses will be described in the topics below.

1.7.1. Bioinert ceramics

These bioceramics do not establish chemical or biological bonds with the living tissue, moving according to the tissue and inducing the formation of a fibrous capsule in the interface material-tissue [110-113]. This movement gradually decreases the functionality of the implant, leading to its replacement [110-112]. The thickness of the fibrous capsule depends on the material and relative movement. The development of implants with small protrusions on its surface allowed a better fixation and decrease of relative movement. This type of fixation is designated as morphological fixation [112].

Some of the most recognized bioinert materials are alumina and zirconia for example [111].

1.7.2. Resorbable ceramics

Resorbable ceramics are known to gradually degrade as time passes, being replaced by living tissue, such as the bone [108,112-115]. There are however, some issues that should be stressed out one of the most important is that this biomaterial should maintain its resistance and stability during the period in which degradation and replacement processes occur. In this line of thought, it is imperative that in order for these bioceramics to be successfully developed, the rate of the degradation should be similar to the rate of the tissue regeneration. [112-114].

Good examples of resorbable ceramics are the calcium-phosphate based ceramics. The chemical composition of these ceramics depends on the ratio Ca/P of the precursors and processing conditions [113].

1.7.3. Porous ceramics

Macroporous bioceramics establish biological bonds with the living tissue that grows in the insides of its pores [110]. This is designated as biological fixation, it's more resistant than the morphological fixation and there's a decrease in the possibility of implant motion [112-114]. These pores must have dimensions superior to 100-150 μm, otherwise vascular tissues essential to tissue growth will not develop. This type of interconnected pores allows blood supply and enables a more effective and healthy tissue growth. On the other hand, porosity diminishes the implant resistance [112-114]. Corals are a very good example of porous biomaterials [111-113].

1.7.4. Bioactive ceramics

A bioactive material is defined as a material with the capacity of developing a specific biological response in the interface material-tissue, resulting in the formation of physical and chemical bonds between the biomaterial and the adjacent tissues [109, 111-116]. The most recognized bioactive materials clinically used are, the bioglasses (Bioglass®), bioactive glass-ceramics (Cerabone A/W®), densified Hydroxiapatite and bioactive composites (PE-HAp; Bioglass®–stainless steel).

The resistance and the mechanism for this bond are individual properties, meaning that these properties depend mainly on the implant material and type of tissue to which it is attached to [101-104], although orientation, age and trial conditions may also play an important role in these mechanisms [112].

Bioglass® and bioglass-type glasses in the form of particulates have gained a lot of successes in periodontal bone repair [117]. Glass-ceramic A-W, owing to its superior mechanical strength and bone-bonding ability, has been applied as artificial vertebrae, intervertebral discs and iliac crests in dense bulk form.

Figure 16 illustrates different bioactive ceramics used in modern medicine.

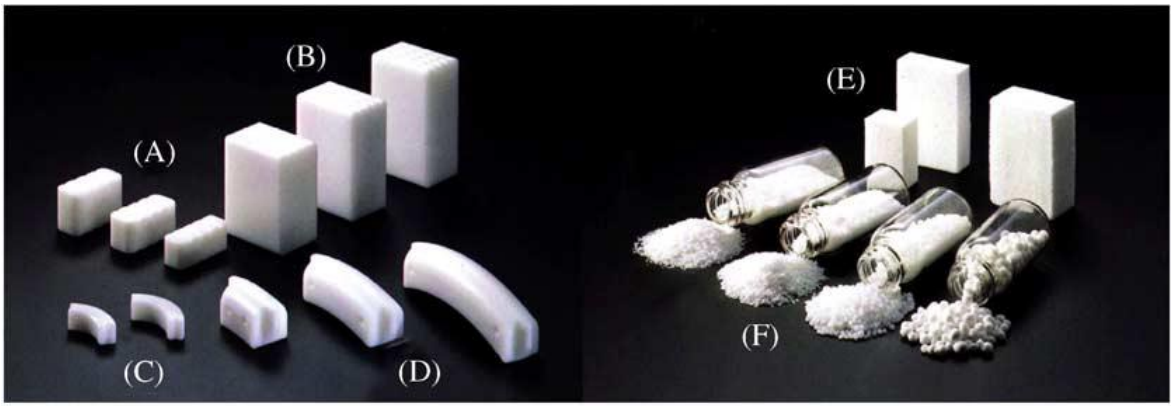

Figure 16 - Glass-ceramic A-W in clinical use: intervertebral discs (A), artificial vertebrae (B), spinal spacer (C), iliac crests (D), porous spacer (E), and bone filler (F). [117]

Also, hydroxiapatite ($Ca_{10}(PO_4)_6(OH)_2$) is one of the most well-known phosphates in the biologically active phosphate ceramic family by virtue of its similarity to natural bone mineral [117].

Synthetic and biological hydroxyapatite has a variety of bioapplications and elicits the formation of an apatite layer at the interface with bone tissue. More on the importance of this apatite will be clarified in the next topic [118-120].

1.8. Bioactivity of a ceramic material in the bone

Histological examinations of bone tissue show that when a bioactive ceramic is in contact with the bone tissue, an apatite layer is formed on the ceramic surface and thereafter, the bone matrix integrates into the apatite [121-124]. Detailed characterization indicates that this apatite layer consists of nano-crystals of carbonate-ion containing apatite rich in Ca and P ions [112,113,115]. These characteristics make in fact, this apatite similar to the mineral phase in bone and, hence, bone cells like osteoblasts, can adhere proliferate, and differentiate on the apatite to form an extracellular matrix composed of biological apatite and collagen [120,125,126].

When this attachment occurs, a chemical bond is formed between the bone mineral and the surface apatite to reduce the interfacial energy between them. In other words, it is suggested that the formation of a layer of biologically active

bone-like apatite in the surface of the ceramic is an essential requirement for an artificial material to bond to living bone.

The *in vivo* formation of an apatite layer on the surface of a bioactive ceramic can be reproduced in a protein-free and acellular simulated body fluid (SBF), which is prepared to have an ion concentration nearly equal to that of human blood plasma, as depicted in Table 2 [117-122].

Table 2 - Ionic concentration of human blood plasma and SBF [117]

	Ionic Concentration (nM)							
	Na^+	K^+	Mg^{2+}	Ca^{2+}	Cl^-	HCO^{3-}	HPO_4^{2-}	SO_4^{2-}
Human plasma	142,0	5,0	1,5	2,5	103,0	27,0	1,0	0,5
SBF	142,0	5,0	1,5	2,5	147,8	4,2	1,0	0,5

Therefore, the *in vitro* bioactivity of an artificial material can be evaluated by examining the formation of apatite on its surface in SBF.

The morphology and composition of the apatite surface layer can be assessed by SEM/EDS, from which it is also possible to estimate the Ca/P ratio in the apatite.

The Ca/P atomic ratio for stoichiometric hydroxyapatite in the bone tissue is 1.667. If this ratio is found in the surface of materials immersed in SBF, it is likely that an apatite formation may be occurring [127,128].

The validity of the immersion tests in SBF to predict the *in vivo* bioactivity of a material was analyzed by Kokubo *et al*. [121]. The authors compiled and compared several studies on bioactivity *in vivo* and formation of the apatite surface layer of materials immersed in SBF and found that. a large group of materials exhibiting the formation of an apatite layer on its surface in SBF also showed to bind chemically to bone *in vivo*. These materials are: Bioglass® 45S5, glass systems Na_2O-CaO-B_2O_3-Al_2O_3-SiO_2-P_2O_5, CaO-SiO_2 and Na_2O-CaO-SiO_2, AW glass ceramics type Ceravital®, calcium sulfate, hydroxyapatite sintered

composite apatite /-TCP and polyethylene / AW-glass ceramic and also metallic oxide gels prepared by sol-gel: SiO_2, TiO_2 and TaO_2. Generally, materials that didn't show *in vitro* formation of apatite in SBF, did not show bioactivity *in vivo*. The phenomenon correlation between *in vivo* and *in vitro* is also quantitative, i.e. the faster the apatite layer is formed in the material *in vitro*, the faster will it bind with the bone tissue *in vivo*. There is at present a consensus on the acceptance that the bioactivity of a material *in vivo* can be predicted from its capability of forming an apatite layer when immersed in a synthetic physiological medium like SBF, provided that the material does not cause major inflammatory reactions or allergies, toxicity or carcinogenesis [122].

2. AIMS AND STRATEGY OF THE DISSERTATION

The combination of cells, engineering, materials, and suitable biochemical and physio-chemical factors to improve or replace biological functions is currently called tissue engineering [129]. Classically tissue engineering is associated with applications that repair or replace portions of the whole tissues [129]. A major current challenge that tissue engineering is facing, is the need for more complex functionality, as well as both functional and biomechanical stability in laboratory-grown tissues for transplantation [130]. The development of selective platforms that will allow directing the organization, growth, and differentiation of cells in the process of tissue formation is then required. Within this context, it has been recently proved the preferential adsorption of proteins to the surface of a polarized piezoelectric biodegradable films [131]. Furthermore, the selective adsorption of biomolecules on charged surfaces and domain boundaries of ferroelectric single crystals of $LiNbO_3$ and $LiTaO_3$ has also been demonstrated [132]. These results open the possibilities to use ferroelectrics as “substrates” for tissue engineering, namely, in devices, which allow the surface charge to be patterned and controlled internally or externally in real time, by simply applying a “force” [131]. However the bioactivity and biocompatibility, key aspects for any bioapplications, of some of these ferroelectrics are not known.

These ferroelectric ceramics have not been studied for biomedical purposes until this date and so, the possible advantages or disadvantages of their piezoelectric and ferroelectric properties combined with the bioelectricity generated by living organisms is unknown.

The main purpose of this research is to study the bioactivity of ferroelectric $LiNbO_3$ and $LiTaO_3$ ceramics. If proved bioactive, these materials can later serve as either a platform to accelerate or to promote the development or regeneration of living tissues, taking advantage of the permanent polarization of a ferroelectric, or as a “bio-actuator”, taking advantage of its piezoelectric nature. These ferroelectric ceramics, if proven biocompatible may even be studied as a potential material to fabricate a catheter or stent for vascular tubes, which may have the

ability to increase or decrease the gap of the vascular lumen. Other biological interactions may also emerge from positive results.

The specific aims of this dissertation are:

1. Preparation of LNO and LTO powders;
2. Characterization of the synthesized powders;
3. Preparation of SBF solution and posterior immersion of the ferroelectric powder samples prepared;
4. Study the respective bioactivity response *in vitro* for each of the powders.

3. MATERIALS AND METHODS

3.1. LNO and LTO powder precursors

For the preparation of LNO and LTO powders, precursors indicated in Tables 2 and 3 were selected.

Table 3 - Chosen precursors for lithium niobate powder synthesis

Compounds	Mass (g)	Purity	Provider
Nb_2O_5	4,5	99%	Merck
Li_2CO_3	1,29	99%	Merck

Table 4 - Chosen precursors for lithium tantalate powder synthesis

Compounds	Mass (g)	Purity	Provider
Ta_2O_5	4,68	99%	Aldrich
Li_2CO_3	0,81	99%	Merck

3.2. Synthesis of LNO and LTO powders

For the preparation of LNO powders niobium pentoxide and lithium carbonate were the chosen precursors (Table 3). Exactly 4,5g of niobium oxide and 1,29g of lithium carbonate were weighted and mixed in order to achieve a ratio of 1:1=$[Li_2CO_3]/[Nb_2O_5]$ + 3% wt. Li_2CO_3 (this wt. 3% of Li_2CO_3 excess was added to compensate possible Li volatilization) for a total of 5g + 3% Li_2CO_3 in weight.

For lithium tantalate synthesis, tantalum pentoxide and lithium carbonate were chosen as precursors (Table 4). Exactly 4,68g of tantalum oxide and 0,81g of lithium carbonate were weighted and mixed with the same analogy used for the LNO powders.

The precursors for both compositions were previously dried for 200°C to reduce the possibility of any unwanted water reaction, due to humidity. Then the precursor powders were both put into 2 teflon jars with 25 zirconia balls and ethanol was added. The jars were taken to a milling machine and the powders were then milled for 8h at 170-180rpm.

After removal, the jars were put into an oven for drying at 120°C for at least 12h, the mixed powders were carefully removed and then calcined at 800°C for 5h. After that, the powders were milled again at 170-180 rpm for 8h to avoid any agglomerates and dried for another 12h before removing it from the teflon jar.

3.3. Characterization of the powders

3.3.1. Particle size distribution and specific surface area measurement

The evaluation of the particle size distribution was done according to the principle of laser diffraction in a Coulter LS Particle Size Analyzer 230 equipment.

The specific surface area of the powders was determined by a technique based on the physical adsorption of gas molecules on a solid surface, developed by Brunauer, Emmett and Teller (BET), using a Micromeritics Gemini 2360 equipment. Before the measurement of the volume of gas adsorbed, the powders remained in vacuum at 200°C for 6h.

3.3.2. Thermogravimetric and differential thermal analysis

The thermogravimetric and differential thermal analysis of the powders were conducted in a Seteram Labsys DTA/TG-DSC equipment, with a heating rate of 10°C/min, from 25 to 1200°C.

The objective of this analysis is to identify the nature of the reactions that may happen during the heat treatment and the respective relevant temperatures of the main transformations, thus investigating the mass variation of the materials as temperature rises.

3.3.3. Microstructural analysis

The microstructural analysis of the LNO and LTO powders was done by SEM using an Hitachi S4100. The sample powders were placed in a plane and polished aluminum sample holder, glued with carbon tape and made conductive by sputtering a carbon layer on the powders surface using in a K950X Turbo Evaporator sputtering equipment.

In a SEM an electron beam is generated inside a vacuum column, this beam is then precisely conducted to the target (surface of the sample) and the electrons are ‘’forced’’ to collide with the sample. An image is possible due to the electronic signal generated by the low angle backscattered electrons, which are created by electron elastic scattering interactions with the material surface [130].

3.3.4. X-ray diffraction

Conventional XRD was used to characterize the crystallography of LNO and LTO powders and these studies were conducted in a Rigaku DMAXIII/C diffractometer from 20 to 70°C. JCPDS/ICDD (Joint Committee on Powder Standards/international Centre for Diffraction Data; Swarthmore, Pensilvânia, USA) data basis was used for the identification of the crystalline phases

3.4. Bioactivity testing technique

In order to test the bioactivity *in vitro* of both LNO and LTO powders a SBF test was conducted.

From the 5g of total powder, 5 samples of 250mg from each powder were separated. The samples were put in the SBF solution and removed at specific timelines (1, 3, 7, 15, 21 days). After being removed from the SBF solution samples and the fluid were characterized by XRD, SEM/EDS, FTIR and Inductively Coupling Plasma Spectrometry (ICPS) and compared, so that a pattern

could be traced. Thus, control samples without immersion were kept for comparison and validation of results.

3.4.1. SBF solution preparation

The SBF solution was prepared following the procedure described by Kokubo *et al.* [121]. The reagents used, source, the purity, the amount used for the preparation of 1 L solution of SBF and the order of introduction in the solution are shown in Table 5.

Table 5 - Display of the order, quantity, supplier and purity of the reagents used for the preparation of 1L SBF [121].

Order	Reagents	Quantity	Provider	Purity (%)
1	NaCl	7.996 g	Panreac	99,5
2	$NaHCO_3$	0.350 g	Riedel-de Haen	99,7
3	KCl	0.224 g	Riedel-de Haen	99,5
4	$K_2HPO_{4.3}H_2O$	0.228 g	Calbiochem	100
5	$MgCl_{2.6}H2O$	0.305 g	Riedel-de Haen	99
6	HCl - 1M	40 ml	Panreac	99
7	$CaCl_{2.6}H2O$	0.548 g	Fluka	99
8	Na_2SO_4	0.071 g	Panreac	99
9	$NH_2C(CH_2OH)_3$	6.057 g	Merck	99,8

The solution was prepared by adding the reagents of 1 to 8 to approximately 700 mL of ultrapure water (Milli Q ®) 36.5 ± 0.5 ^{0}C under constant stirring. Each reagent was slowly added and after complete dissolution of the previous one in

order to avoid possible precipitation. The solution must remain transparent and the temperature should be approximately 36.5 ± 0.5 ^{0}C. The reagent 9 allows the adjustment of the pH, thus reactant 9, tris-hydroxymethyl aminomethane (Tris) was added to the solution very slowly (during approximately 1 hour) because the rapid increase of pH caused by its addition may provoke precipitation of calcium phosphate. Ultrapure water was added to complete the 1000 ml solution.

3.4.2. Immersion conditions

For bioactivity testing using SBF, each test consisted of dispersing 250 mg of each of the powders in 10 ml of SBF solution.

The powders were deposited in the flask before the SBF liquid, in order to minimize the dispersion of the solid particles. All flasks were put into an incubator at 37°C and one flask from each composition was removed after 1, 3, 7, 15 and 21 days of immersion in SBF. After removing from the incubator, the powders are properly filtered and kept drying for at least 2 days before examined for bioactivity.

The liquid that was removed with the syringe was kept in a refrigerator at 6ºC for further ICPS testing in order to evaluate possible existing ionic exchanges between the powders and the SBF environment, which can be treated as a solvent.

3.5. Bioactivity characterization techniques

In order to conclude that the material is bioactive in vivo there are certain scientific tests that should be used to clarify the bioactivity of the samples after the immersion of the material in SBF.

3.5.1. SEM-EDS

A detailed microstructural analysis of the immersed powders was made by SEM/EDS searching for the existence of a calcium-phosphate apatite that traditionally looks like a cauli-flower.

The SEM is equipped with a microanalysis system for energy dispersive spectrometry of X-rays/EDS. The EDS analysis involves the generation of an X-ray spectrum from the entire scanned area of the SEM that displays the major elements present in the material and their intensity. The EDS software associates the energy level of the X-rays with the elements of the periodic table. In this way the Ca/P atomic ratios were also calculated from the EDS.

3.5.2. X-Ray Diffraction

The crystallographic characterization of the immersed powders was made through the same technique utilized in 3.3.4.

3.5.3. Fourier Transform Infrared Spectroscopy

FTIRM-ATR was used to obtain an infrared spectrum of absorption of the powder, it collects spectral data in a wide spectral range, and it measures how well a sample absorbs light at each wavelength used in the testing.

An attenuated total reflection accessory (ATR) operates by measuring the changes that occur in a totally internally reflected infrared beam when the beam comes into contact with a sample. An infrared beam is directed onto an optically dense crystal with a high refractive index at a certain angle. This internal reflectance creates a wave that extends beyond the surface of the crystal into the sample held in contact with the crystal.

Fourier Transformed Infrared Attenuated Total Reflectance Microscopy (FTIRM-ATR) studies were performed using a FT-Infrared Broker Optics – Tensor

27 operating in Attenuated Total Reflectance mode (Golden Gate®) from 200 to 4000 cm^{-1}.

3.5.4. Inductively coupled plasma

The SBF solution and the residual SBF liquid from each immersed sample (preserved at ~4-6°C) was characterized by emission spectroscopy induced plasma (ICP) in a Jobin-Yvon JY70 Plus, France, in the Central Analysis Laboratory of University of Aveiro, that allowed to analytically determine the elemental concentration of the solutions.

4. RESULTS AND DISCUSSION

This section will present and discuss the results obtained for the studies conducted on the bioactivity of lithium niobate and lithium tantalate powders.

The chapter starts by discussing the thermic behavior of the mixed powders (DTA/TG) and the crystallographic characterization of the calcined powders (XRD). Then analysis the morphological study carried out on the powders (Particle size distribution, BET and SEM of the non-immersed powders) and finally presents the results and characterization of the bioactivity tests (SEM/EDS, XRD, FTIR-ATR and ICP).

4.1. Thermic behavior analysis

The results of TG and DTA measurements at 10°C/min for lithium niobate are shown in Figure 17

The largest mass lost (approximately 13%) is observed between 350^{0}C and 680^{0}C, which may be attributed to the decomposition of the precursors, namely the carbonates with the release of CO_2, stabilizing until 1200^{0}C, as no significant weight loss is observed at temperatures higher than 680^{0}C.

The main peak of the DTA curve is an exothermic one that appears at 700-720^{0}C, that mainly corresponds to the ending of the weight loss and is assigned to the crystallization of $LiNbO_3$. This is in accordance with the results of the TG analysis, as the $LiTaO_3$ formation reaction mainly occurs upon the decomposition of the precursors, in this case above 680^{0}C. It is also an indication of the minimum calcination temperature to produce high quality $LiNbO_3$ powders.

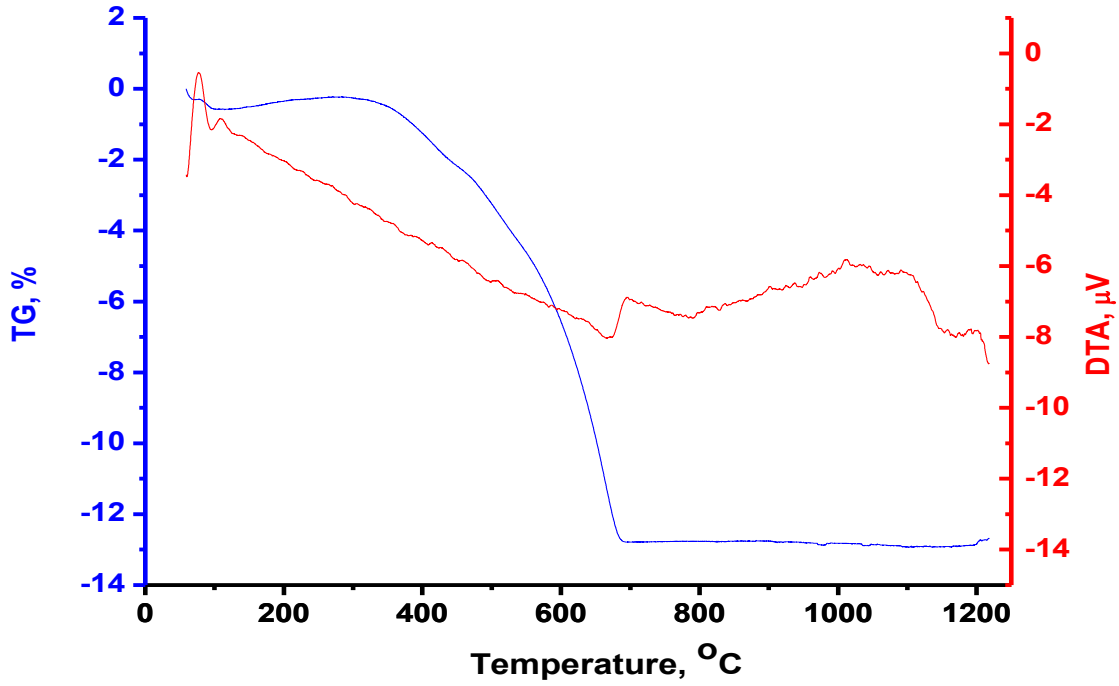

Figure 17 - DTA and TG curves for Lithium niobate powder. DTA is denoting the exothermic and endothermic changes in the sample throughout the elevation of the temperature and TG is denoting the changes in weight as temperature increases from room temperature to 1200°C.

The results of TG and DTA for lithium tantalate are shown in Figure 18.

Similarly to LNO powders the largest mass lost (approximately 9%) is observed between 410^{0}C and 625^{0}C, which may be attributed decomposition of the precursors, namely the carbonates with the release of CO_2, then it stabilizes until 1200^{0}C as no significant weight loss is observed at higher temperature than 625^{0}C.

The correspondent DTA curve is mainly characterized by an exothermic peak at about 620^{0}C, which coincides with the ending of the weight loss and is assigned to $LiTaO_3$ powder crystallization. This is in accordance with the results of the TG analysis, as the $LiTaO_3$ formation reaction mainly occurs upon the decomposition of the precursors, in this case above 620^{0}C. This is also an indication of the minimum calcination temperature to produce high quality $LiTaO_3$ powders.

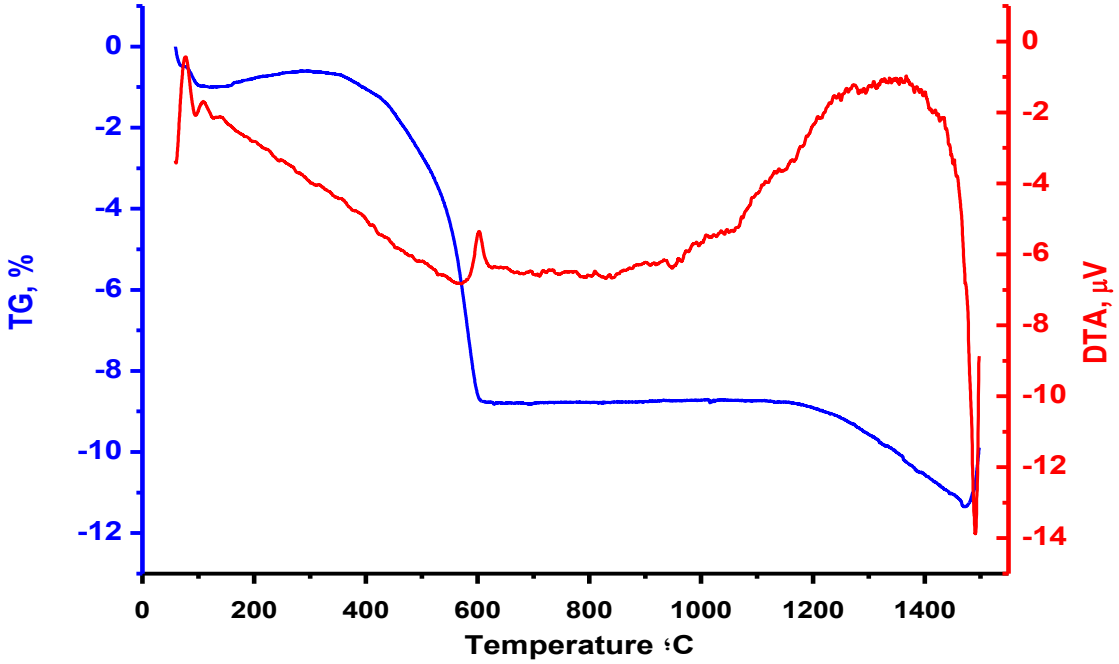

Figure 18 - DTA and TG curves for Lithium tantalate powder. DTA is expressing the exothermic and endothermic changes in the sample throughout the elevation of the temperature and TG is expressing the changes in weight as temperature increases from room temperature to 1500°C

Figure 19 illustrates the XRD patterns of the powders calcined at 800°C for 5h. According to the JCPDS card of lithium niobate (JCPDS #01-020-0631 $LiNbO_3$), all the diffraction peaks can be attributed to the trigonal crystal structure of $LiNbO_3$ and no second phases or impurities are found after calcination. These results are in agreement with the DTA/TG results..

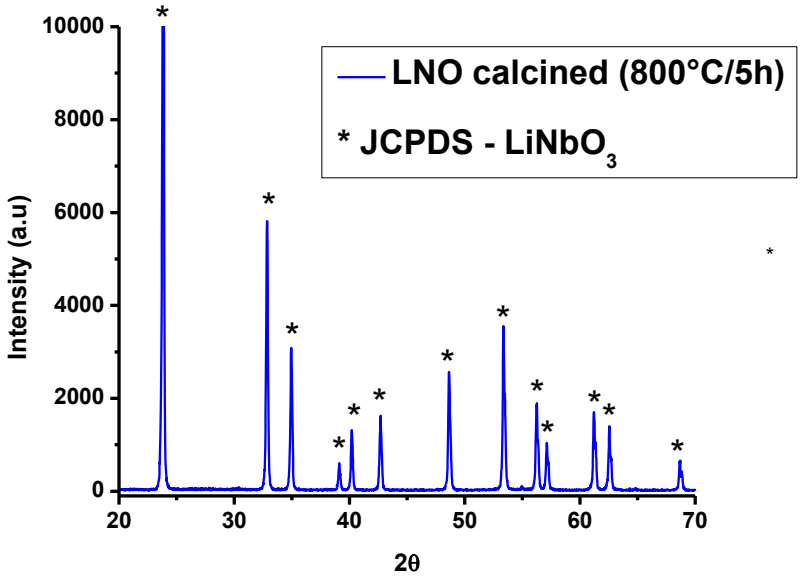

Figure 19 - XRD pattern of lithium niobate powders calcined at 800ºC. The pattern reveals a monophasic material at this temperature.

Figure 20 illustrates the XRD patterns of the powders calcined at 800°C for 5h. According to the JCPDS card of lithium tantalate (JCPDS #01-088-0290 $LiTaO_3$), all the diffraction peaks can be attributed to the trigonal crystal structure of $LiTaO_3$ and no second phases or impurities are found after calcination. These results are also in agreement with the DTA/TG results.

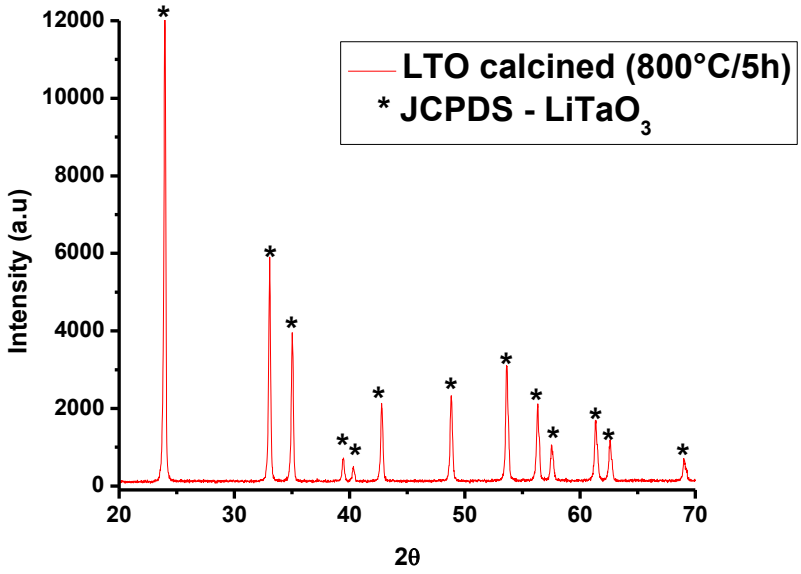

Figure 20 - XRD patern of lithium tantalate powders calcined at 800ºC. The pattern reveals a monophasic material at this temperature.

4.2. Morphology and particle size analysis of LNO and LTO calcined powders

The particle size distribution of LNO powders after milling and calcination is represented in Figure 21. Characterized by two peaks, one centered around 3 µm and another one below 1 µm, the mean particle size at 50% vol. of the distribution is 1.918 µm. The specific surface area by BET technique was determined to be 0,8991 m^2/g.

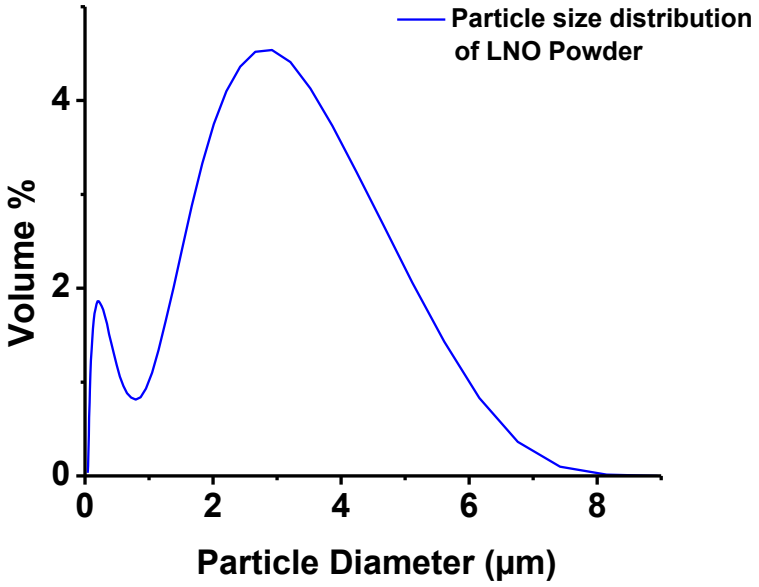

Figure 21 - Particle size distribution for lithium niobate powders with a clear bimodal distribution.

For the case of LTO powders (Figure 22) a similar particle size distribution was obtained. It's possible to observe a large distribution, with particles ranging between 0,115~3,535 µm, with a mean particle size at 50% vol. of the distribution of 1.451 µm. For these powders the BET specific surface area was determined to be 1,6732 m^2/g.

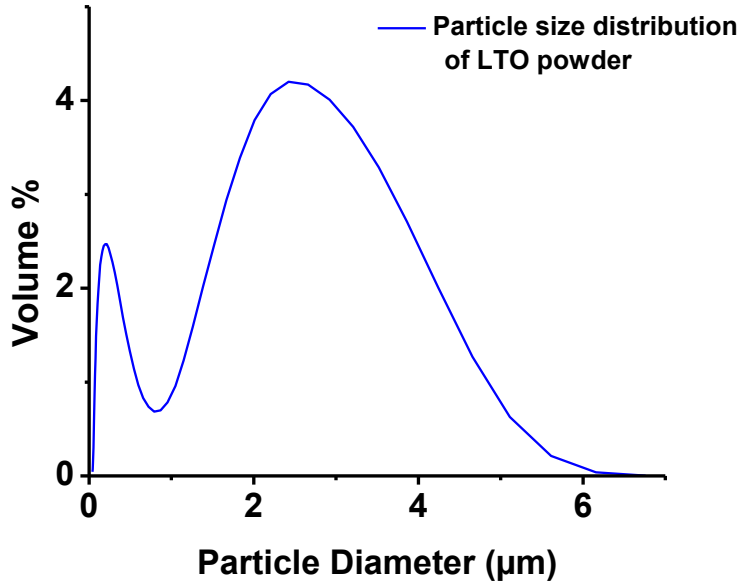

Figure 22 - Particle size distribution for lithium tantalate powders with a clear bimodal distribution.

Figure 23 and 24 presents the SEM micrographs of lithium niobate and lithium tantalate powders after calcination and milling.

In agreement with the previous morphology data LNO present a slightly bigger particle size than LTO powders. The obtained powder morphology is similar to the one obtained by Kuo C. *et al*. (Figure 14a) for LNO powders prepared by combustion method. The same can be said for LTO powders when comparing with the microstructures reported by Zheng F. *et al*. (Figure 16) for LTO powders prepared by hydrothermal and wet-chemical route.

A)

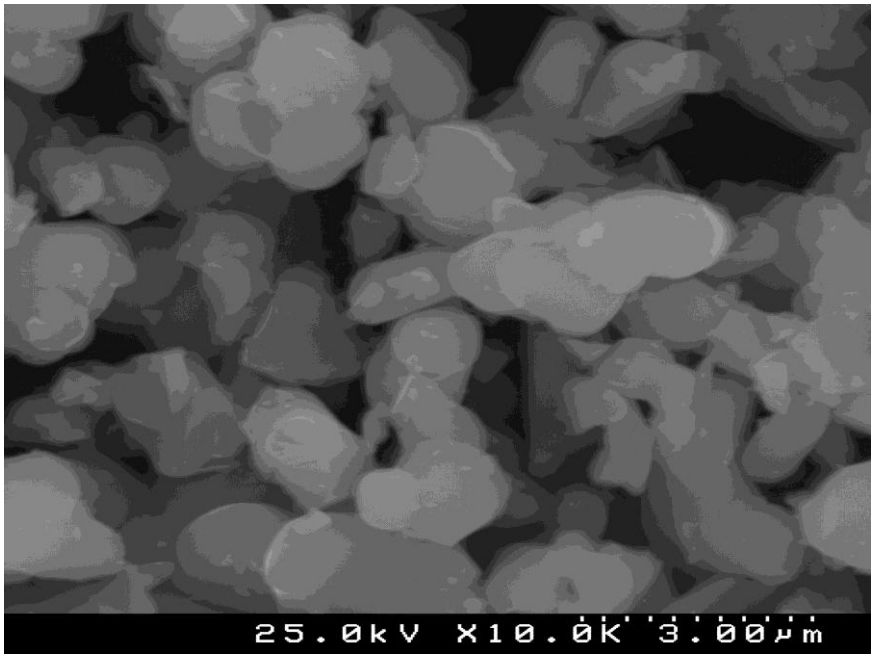

B)

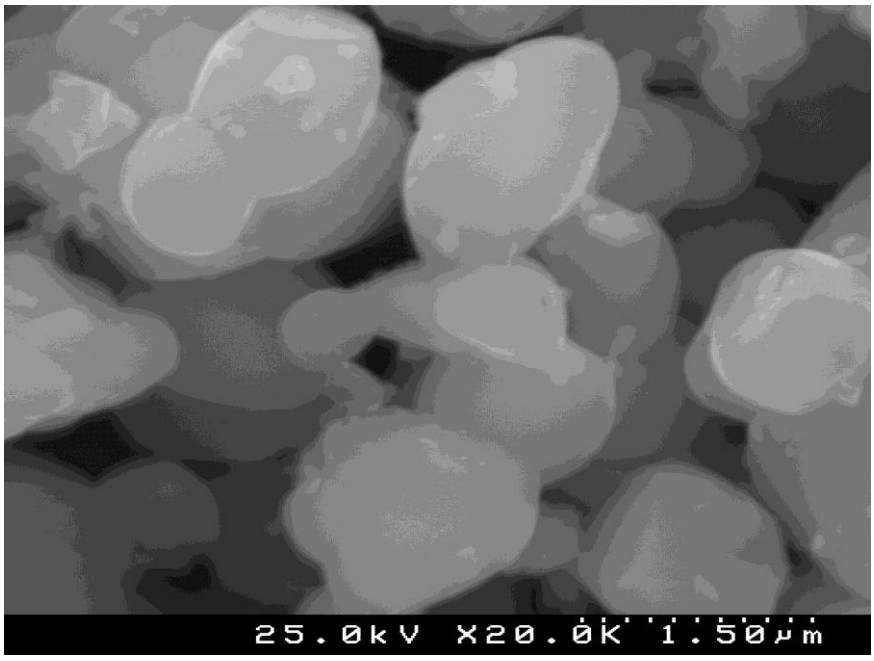

Figure 23 - SEM micropgraphs of lithium niobate powders after calcination and milling .A) 10 K magnification and B) 20 K magnification.

A)

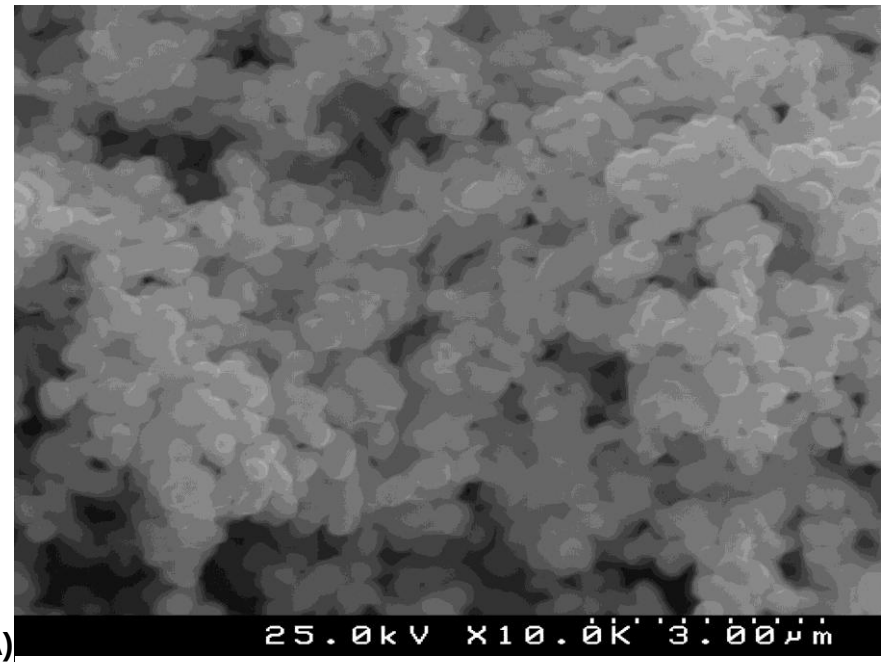

B)

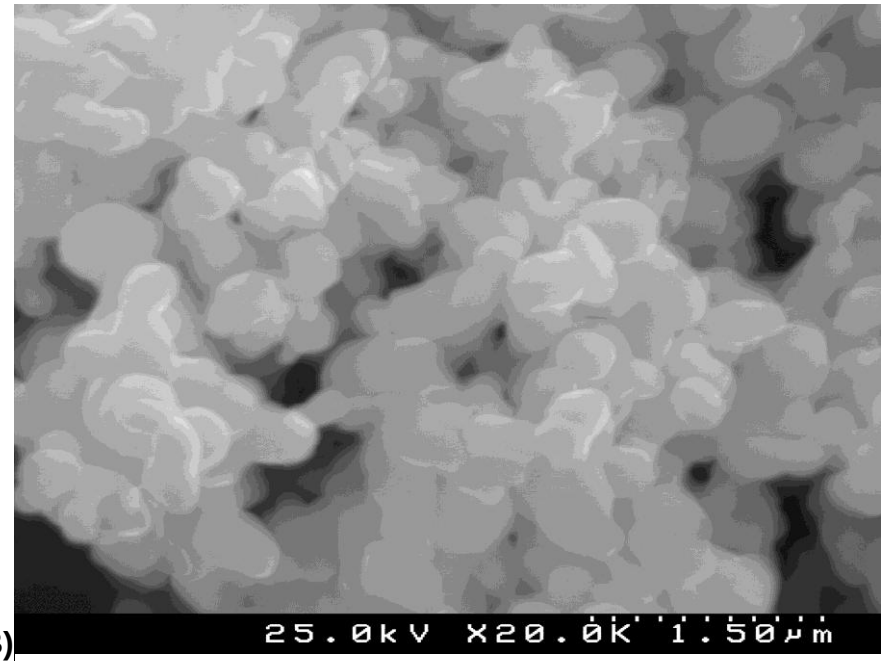

Figure 24 - SEM micropgraphs of lithium tantalate powders after calcination and milling .A) 10 K magnification and B) 20 K magnification.

4.3. Powder studies after SBF immersion

4.3.1. X-ray Diffraction

Regarding the XRD characterization of the immersed powders, a JCPDS card of HAp was added to the plotted graphs in order to compare the peaks from the synthesized powders with the ones of the reference file of Hap, as a way to give clues regarding the formation on the surface of the powders of calcium phosphate.

Figure 25 presents the XRD patterns of $LiNbO_3$ powders after immersion in SBF. In this figure is also included the spectra of the powders not immersed, as a comparison. Independently on the immersion time, all the spectra exhibit very well defined peaks that correspond to the LNO structure and no extra peaks are present. If there was the formation of any Hap phase during the immersion in SBF fluid it is not detected by XRD. No secondary phases corresponding to the apatite were found from comparison with the JCPDS card of the HAp (JCPDS 073-0293) and no valid conclusion regarding the powders bioactivity can be extracted from these results.

The X-ray diffraction analysis of the $LiNbO_3$ powders before immersion in SBF exhibited a XRD pattern with strong and thin peaks. These peaks position and line-widths corresponded to a well-crystallized $LiNbO_3$ (JCPDS 020-0631), as shown in Fig.19.

The same can be said for the patterns related to the powders that were submitted to the SBF soaking as no differences in the peaks position and peak widths are observable.

It can also be said that, from the analysis of the XRD patterns of the $LiNbO_3$ powders that were immersed in SBF that, no secondary phases corresponding to the apatite were found from comparison with the JCPDS card of the HAp (JCPDS 073-0293) and no valid conclusion regarding the powders bioactivity can be pulled out from the plotted graph.

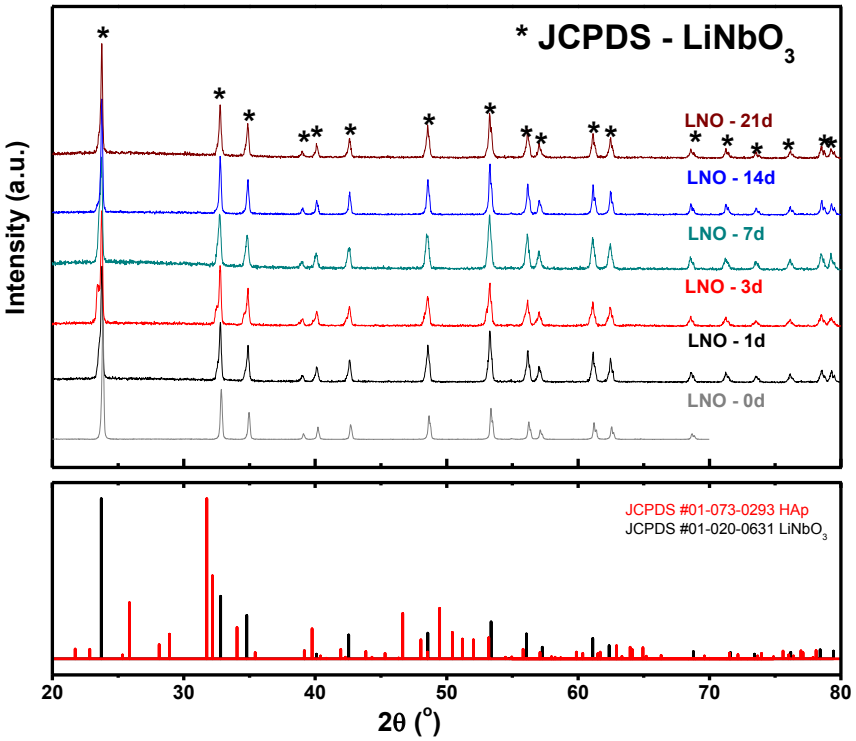

Figure 25 - XRD patterns of lithium niobate powders on top after immersion in SBF for 0, 1, 3, 7, 15 and 21 days. In the bottom there is a representation of the JCPDS patterns for lithium niobate and hydroxyapatite for comparison with the peaks from XRD patterns of the synthesized powders.

Concerning the tantalate powders (Figure 26) similar conclusions to the LNO powders behavior can be drawn. No secondary phases can be detected in these XRD spectra for any of the SBF immersion times.

No conclusive observations regarding the powders bioactivity can be pulled out from these results.

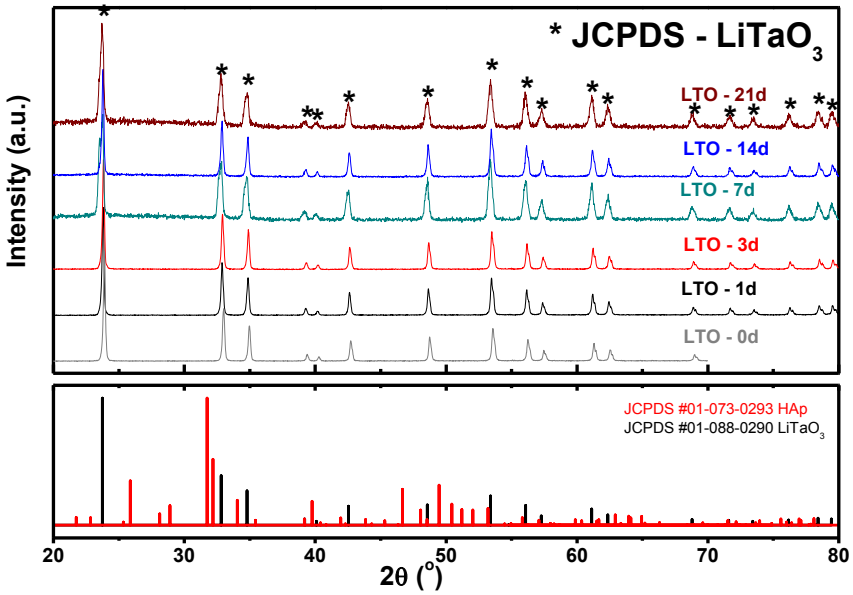

Figure 26 - XRD patterns of lithium tantalate powders on top after immersion in SBF for 0, 1, 3, 7, 15 and 21 days. In the bottom there is a representation of the JCPDS cards for lithium tantalate and hydroxyapatite for comparison with the peaks from the XRD patterns of the fabricated powders.

In Figure 27 we can see a similar attempt realized by Zhou Z. *et al*. that attempted to demonstrate the significance of this comparison of HAp and PLLA patterns. In Zhou Z. *et al*. experiment, PLLA was also immersed in SBF for several days.

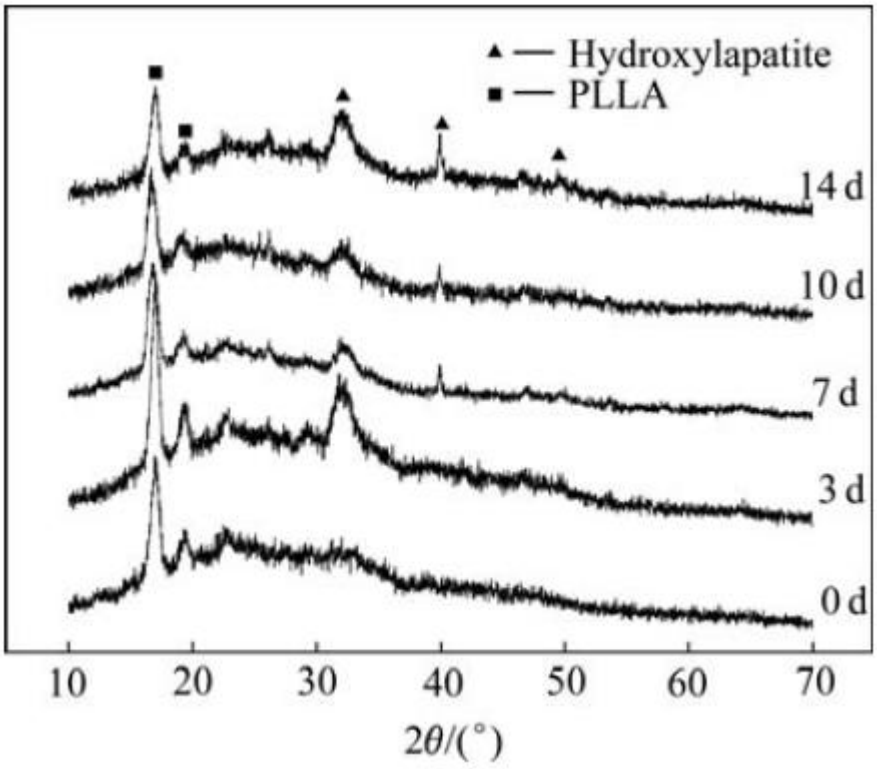

Figure 27 - XRD patterns of PLLA/bioactive glass before and after soaking in SBF [134]

4.3.2. SEM/EDS analysis of the immersed powders

The morphology of LNO and LTO powders immersed in SBF for 1, 3, 7, 15 and 21 days was further analyzed by SEM/EDS and compared either with the unsoaked powders morphology of this study or morphologies reported in the literature for materials in which HAp has been developed during soaking in SBF.

. As stated in the introduction of the thesis (Chapter 1.8), if the powder is bioactive it will react with SBF and apatite-like structures based on calcium-phosphate will be formed.

.

4.3.2.1. Morphology analysis of Lithium Niobate powders by Scanning electron microscope

The surface morphology of $LiNbO_3$ powders after immersion in SBF for 0, 1, 3, 7, 15 and 21 days was carefully examined by SEM.

For soaking times below 15 days there is no obvious modification of the microstructure. *i.e*. there are no evidences for the formation of elongated particles appearing like cauliflowers suggesting the formation of apatite-like particles.

However, for the powders soaked for 15 and 21 days in SBF (Figures 29 and 31) particular elongated particles are clearly visible that resemble apatite-like particles suggesting the formation of deposits of calcium phosphate in these samples.

Since there are no studies on the microstructure of SBF immersed lithium niobate or lithium tantalate materials, the observed structures are compared with for example fluorapatite elongated particles growth in gelatin matrices as represented in Figure 39. The resemblance of the microstructures supports the formation of Hap in LNO powders immersed in SBF for more than 15 days [135].

For a further confirmation EDS was conducted and the spectra plotted for the samples immersed in SBF for 7, 15 and 21 days. For LNO powders immersed in SBF for 7 days (Fig. 28), there are no clear peaks of calcium or phosphate, suggesting that at this point, no apatite-like structures have been formed, confirming the SEM observations. However from the EDS in Figure 30 Ca and P peaks are clearly visible in the spectra of the powder soaked for 15 days. Also, small peaks attributed to Cl and Na are present and these may come from the SBF itself. The Ca/P atomic ratio is in this case 1,84, which is very close to the value of calcium phosphate apatites in HAp (Ca/P ratio of HAp in bone = 1,67 [127, 128]). These observations are in agreement with the SEM ones.

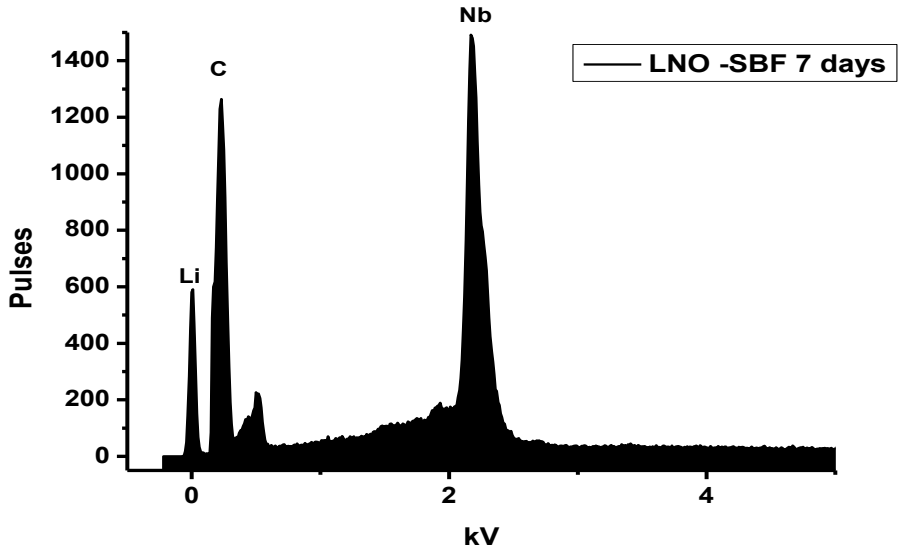

Figure 28 - EDS graph showing the elemental peaks present in the LNO powder sample that was immersed in SBF for 7 days.

A)

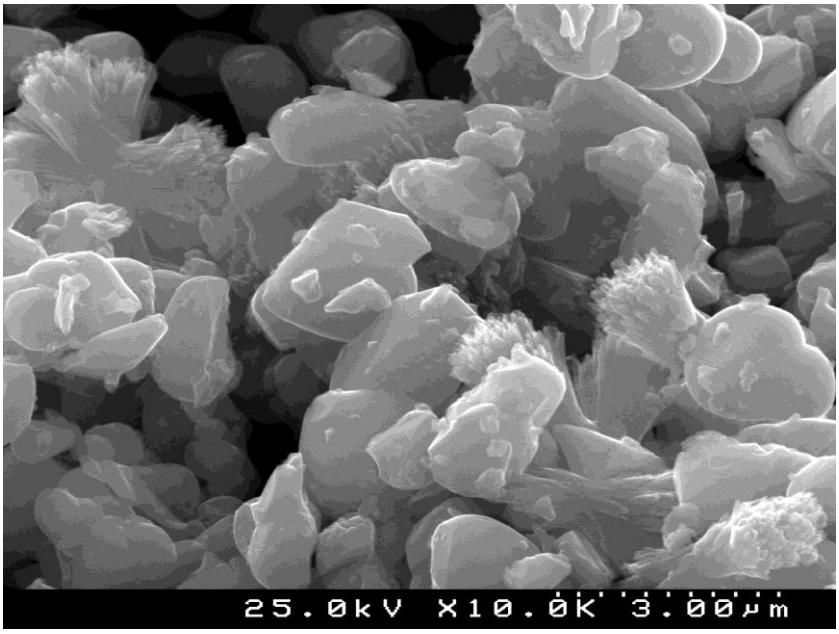

B)

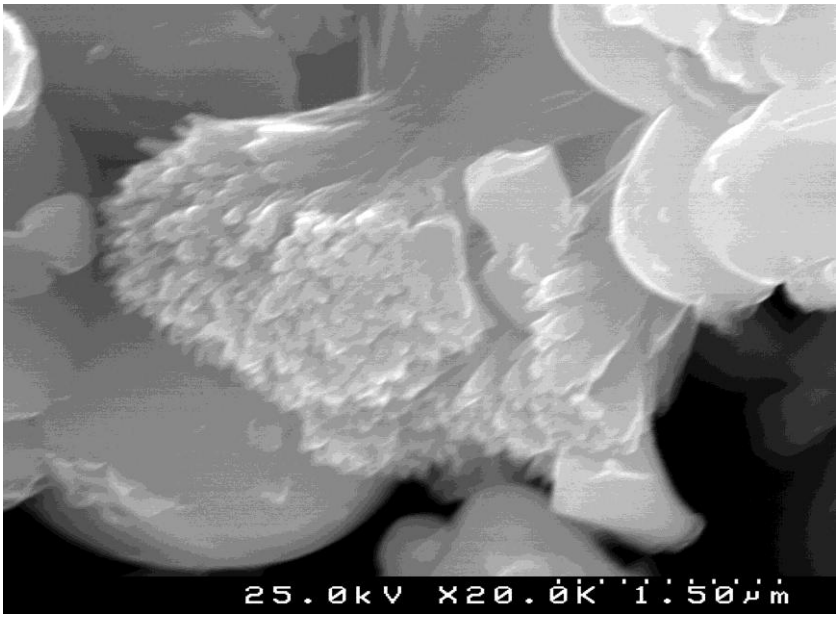

Figure 29 – SEM micrographs of apatite-like structures in lithium niobate powders after soaking in SBF for 15 days with A) 10 K magnification and B) 20 K magnification

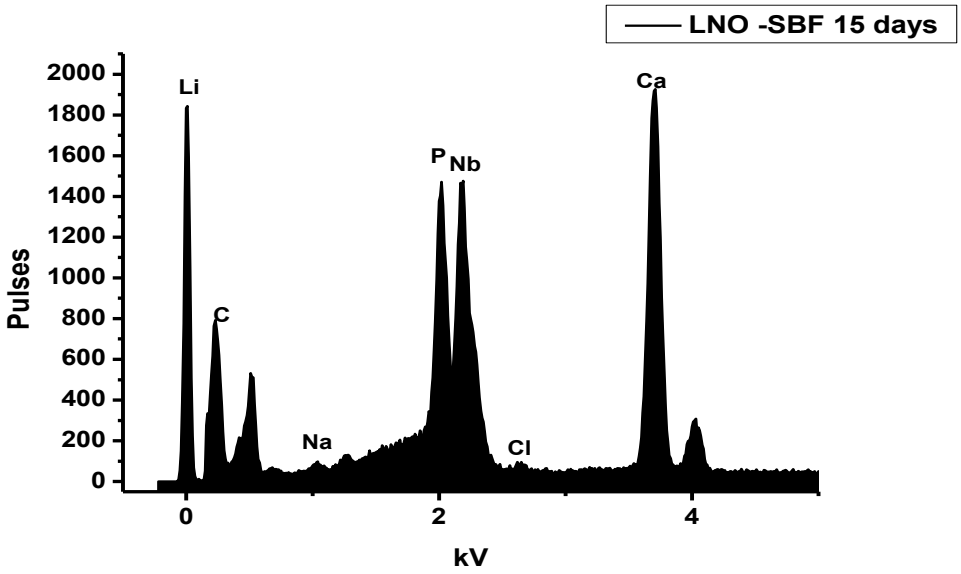

Figure 30 - EDS graph showing the elemental peaks present in the LNO powder sample that was immersed in SBF for 15 days.

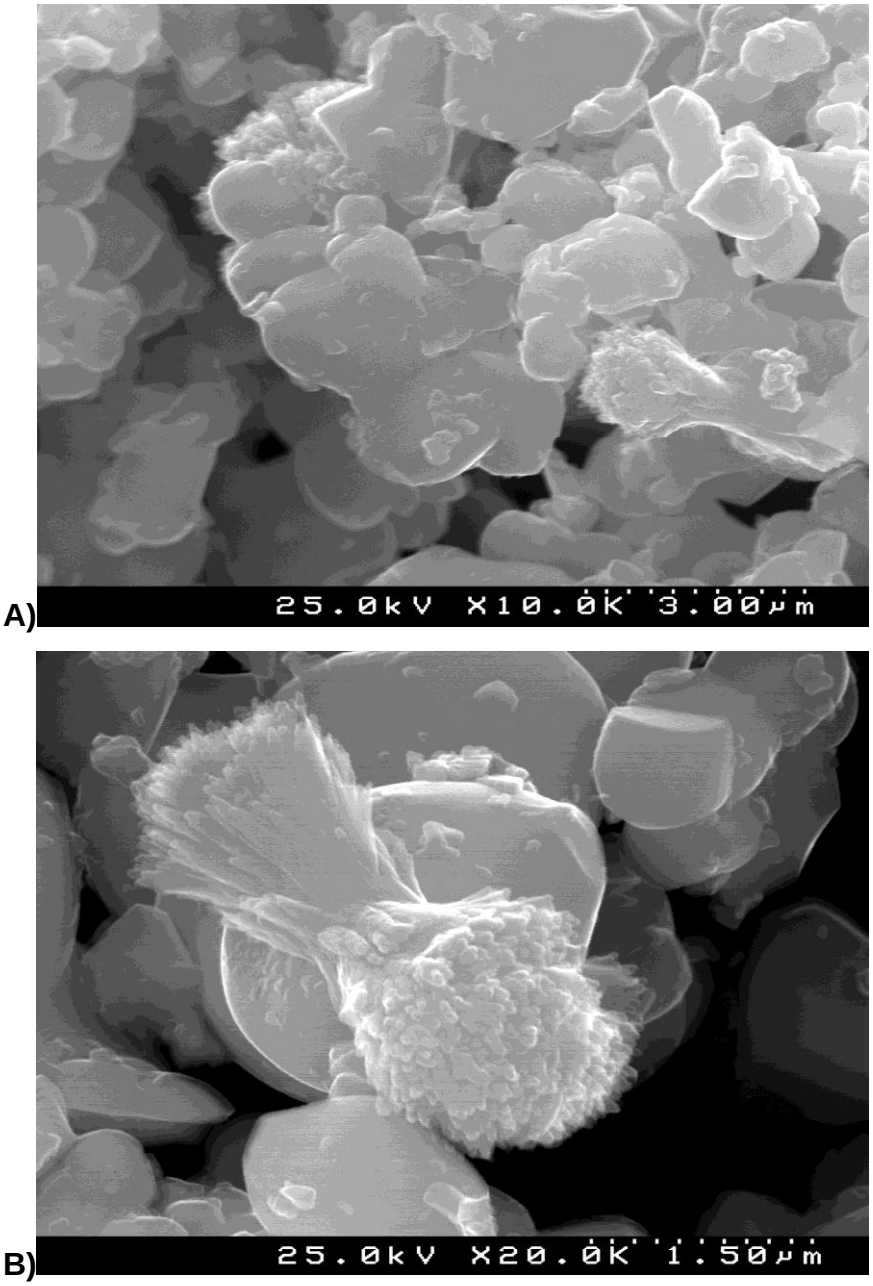

Figure 31 - Representation of SEM images of apatite-like structures in lithium niobate powders after soaking in SBF for 21 days with A) 10 K magnification and B) 20 K magnification.

In Figure 32 the EDS spectrum of LNO powders incubated for 21 days in SBF is represented showing major peaks of Ca and P, confirming the formation of calcium-phosphate particles at the surface of LNO powders indicative of a possible biological response with living tissues *in vivo*. Calculating the Ca/P atomic ratio for this powder, it was determined as 1.65, which is the ideal value for good quality

apatite formation; apatites that have its ratio near this valor appear to form a stronger bond with the tissue [127, 128].

In Table 6 there's a verification of the calculus realized with the Ca/P ratios for the tested LNO powders.

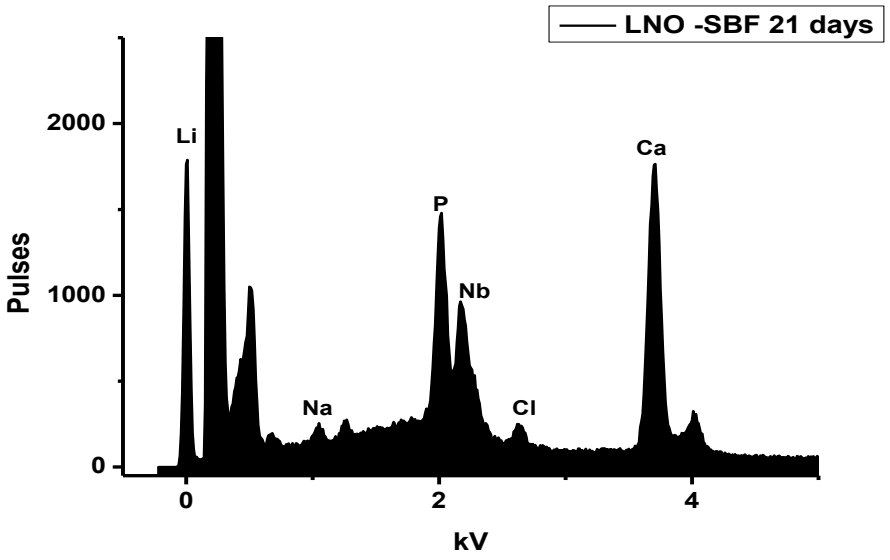

Figure 32 - EDS graph showing the elemental peaks present in the LNO powder sample that was immersed in SBF for 21 days.

Table 6 - Ca/P ratio calculated for LNO powders after immersion in SBF for 7, 15 and 21 days.

Lithium niobate in SBF (day)	Ca (mol)	P (mol)	Ca/P atomic ratio
7	0,12	2,24	N/D
15	16,77	9,12	1,84
21	6,88	4,18	1,65

4.3.2.2. Morphology and grain size analysis of Lithium Tantalate powders by Scanning Electron Microscopy

The surface morphology of $LiTaO_3$ powders after immersion in SBF for 0, 1, 3, 7, 15 and 21 days was analyzed by SEM equipment. The samples of day 1 and 3 are not depicted as no significant changes were found in its surface in comparison with the 0 day sample.

In the case of lithium tantalate powders, it is observable that elongated particles have formed within 7 days of immersion in SBF (Fig. 33). In the EDS graph measurements for the LTO powder that was immersed in SBF for 7 days (Fig. 34), it is detected a high peak capture of Ca and there's also a small peak for P. This might reinforce the fact that at this point calcium-phosphate nuclei might be forming.

The Ca/P for this sample is approximately 1,91, which suggests that at this stage, a high quantity of Ca has been provided by the SBF to the surface of the powder and thus leading to the formation of a calcium phosphate which is phosphorus deficient when compared to hydroxyapatite [127, 128].

From the images related to the 15 and 21 days soaking of lithium niobate powders, it is even more clear that particular elongated apatite particles have been formed on the surface of the powders (Figures 41 and 43 respectively). thus suggesting the capability of this ferroelectric ceramic to behave as bioactive *in vivo*.

In the LTO powders immersed for 15 days, the EDS shows clear Ca and P peaks and also, small peaks of Cl^- and Na^+ are present and these also come from the SBF (Fig. 42).

These peaks reinforce the fact that calcium-phosphate precipitates have formed on the surface of LNO powder expected to induce a biological response *in vivo*, The Ca/P atomic ratio is in this case 1,00, which represents a sunstantial decrease in this valor. This might mean that the quality of the apatite formations may not be as similar to that of HAp as the one noticed with the lithium niobate powders.

A)

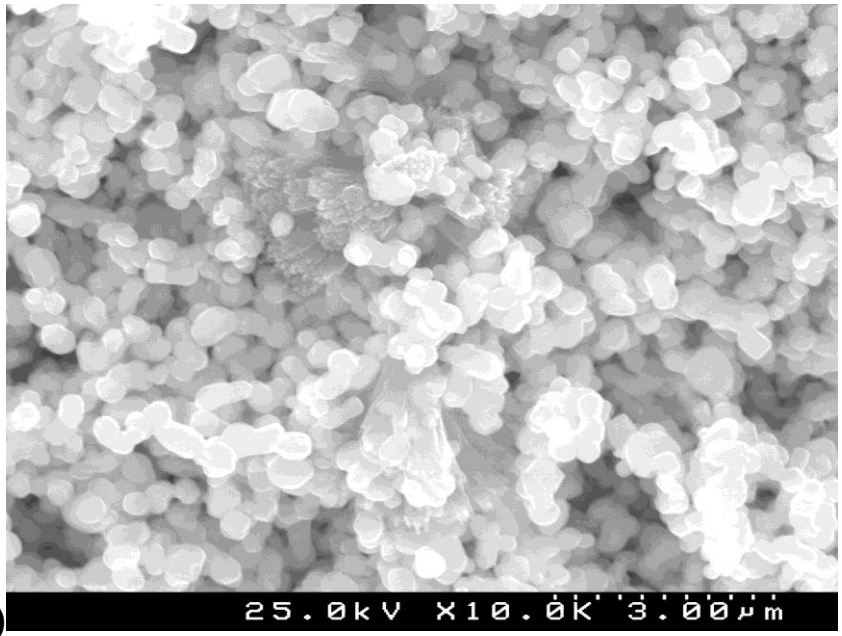

B)

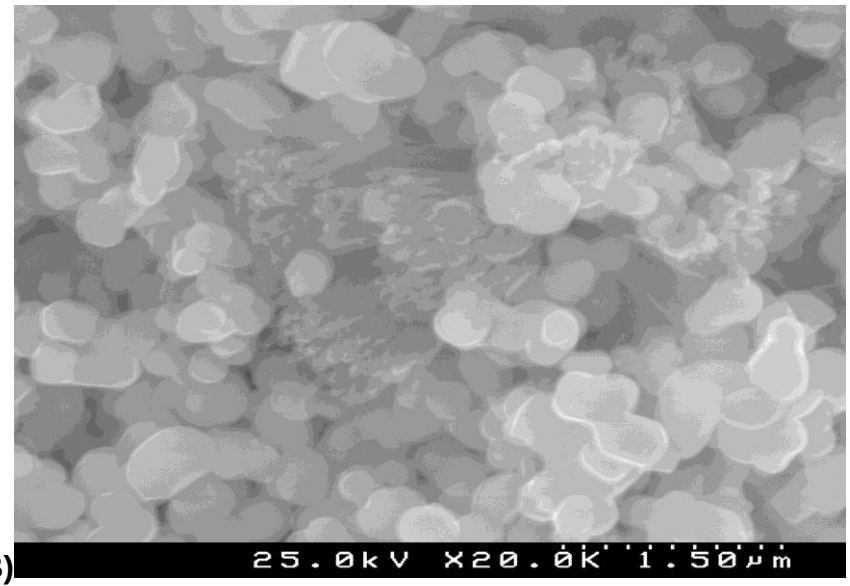

Figure 33 - Representation of SEM images of apatite-like structures in lithium tantalate powders after soaking in SBF for 7 days with A) 10 K magnification and B) 20 K magnification

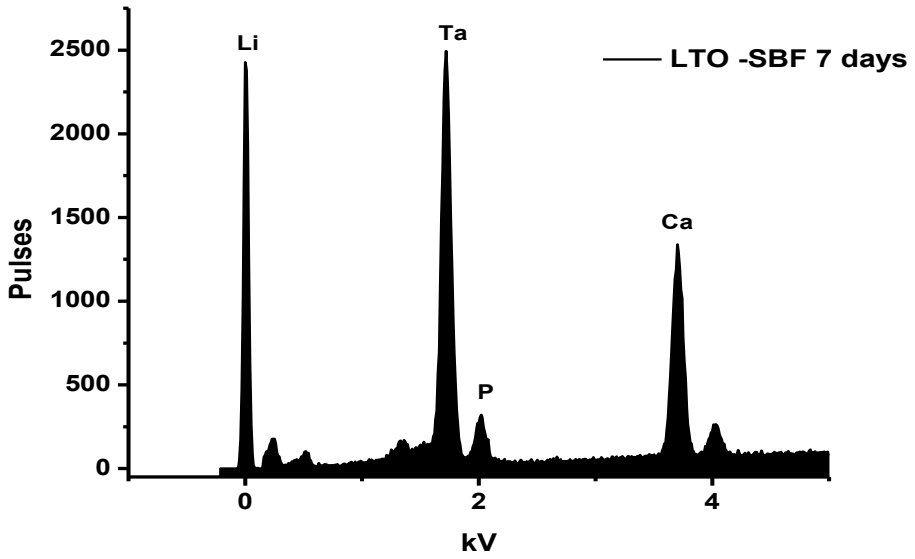

Figure 34 - EDS graph showing the elemental peaks present in the LTO powder sample that was immersed in SBF for 7 days.

A)

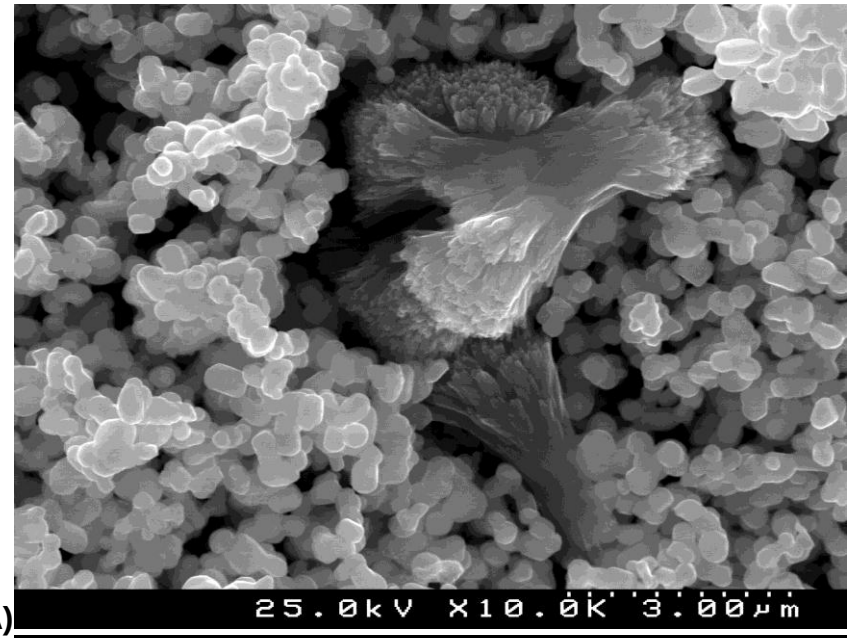

B)

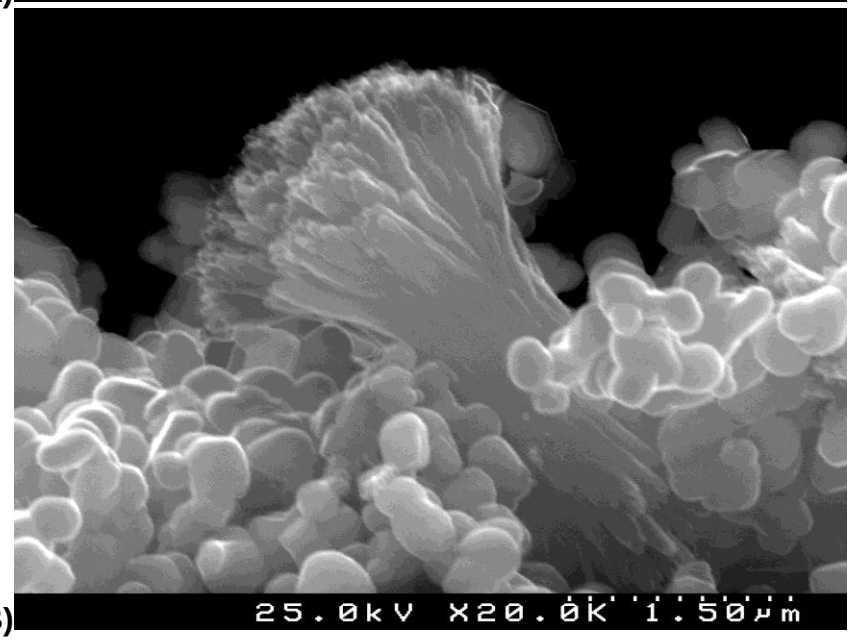

Figure 35 - Representation of SEM images of apatite-like structures in lithium tantalate powders after soaking in SBF for 15 days with A) 10 K magnification and B) 20 K magnification

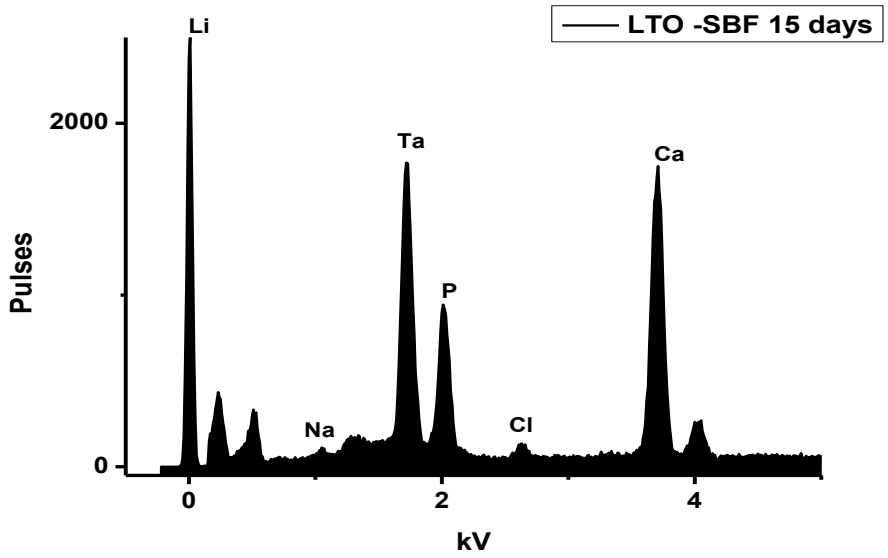

Figure 36 - EDS graph showing the elemental peaks present in the LTO powder sample that was immersed in SBF for 15 days.

A)

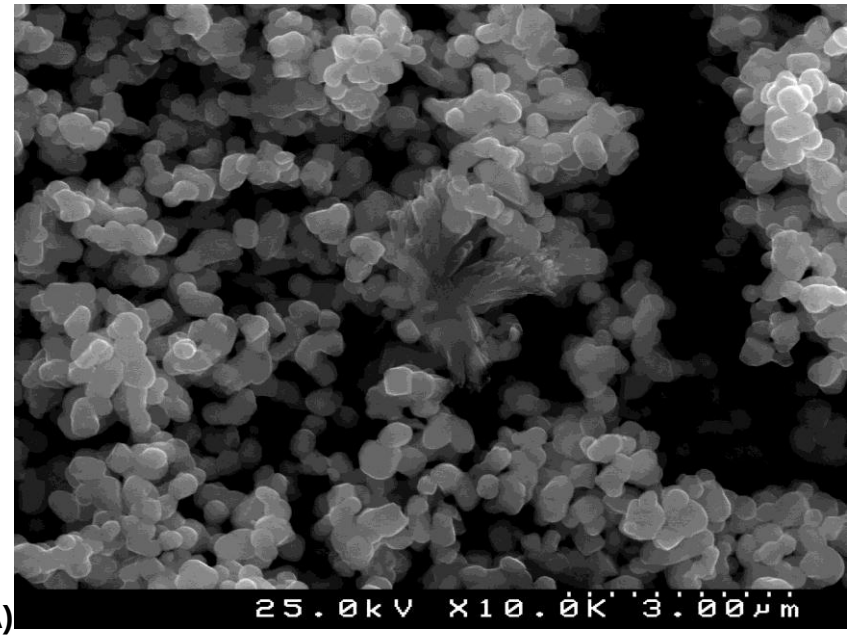

B)

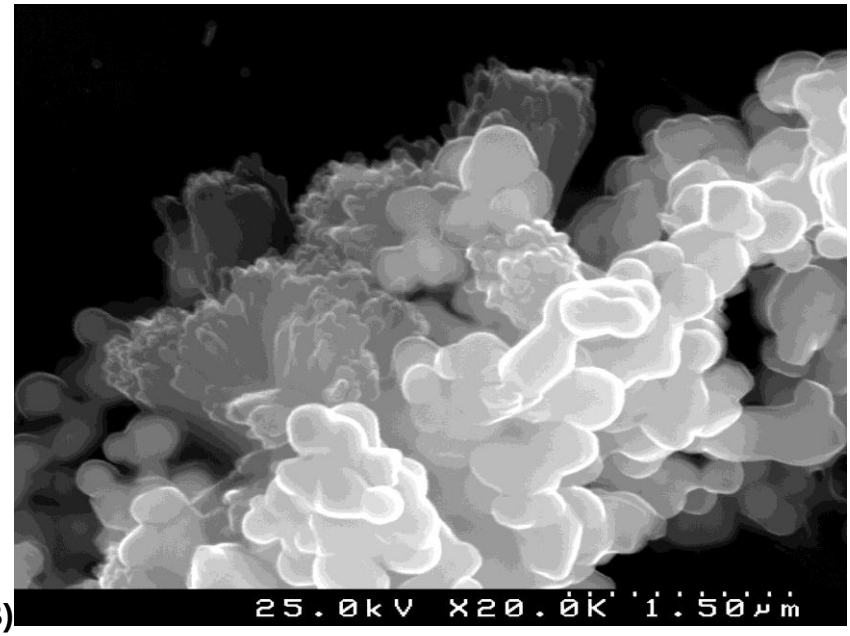

Figure 37 -Representation of SEM images of apatite-like structures in lithium tantalate powders after soaking in SBF for 21 days with A) 10 K magnification and B) 20 K magnification

The EDS spectrum for 21 days immersion of LTO synthesized powders also shows high peaks of Ca and P, proving that these elements are easily detected in the SEM scanned area and bioactivity of the powder is then suggestive., The Ca/P atomic ratio for the 21 days LTO sample is very low: 0.68.

In Table 7 there's a verification of the calculus realized with the Ca/P ratios for the tested LTO powders

By the analysis of the Ca/P atomic ratios, a pattern can be formulated, indicating that the Ca/P atomic ratios have been decreasing from 7 days to 21 days, suggesting that the chemical composition of the precipitated calcium phosphate is moving away from that of the stoichiometric hydroxyapatite.

.

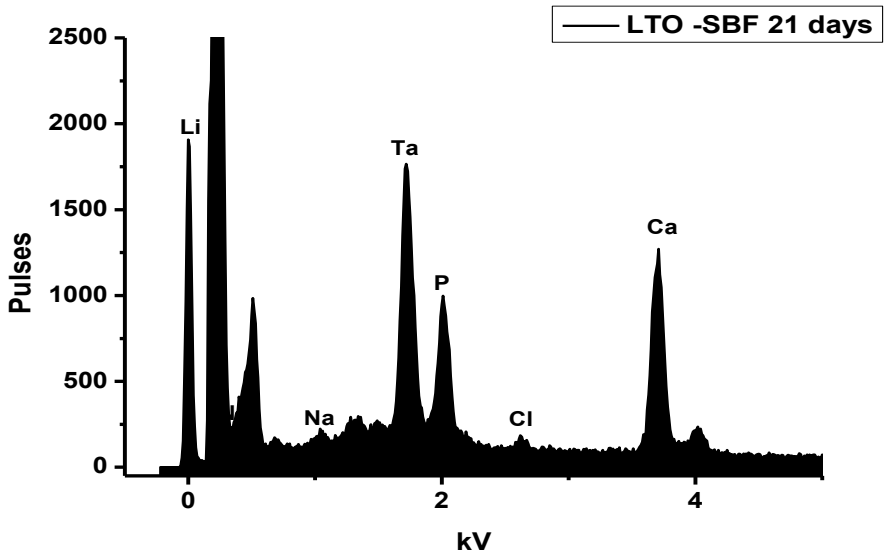

Figure 38 - EDS graph showing the elemental peaks present in the LTO powder sample that was immersed in SBF for 21 days.

Table 7 - Ca/P ratio calculated for Lithium Tantalate powders after immersion in SBF for 7, 15 and 21 days.

Lithium tantalate in SBF (day)	Ca (mol)	P (mol)	Ca/P atomic ratio
7	39.02	20.47	1.91
15	36.08	36.06	1,00
21	34.71	51.12	0.68

In Figure 39 there's a micrograph of fluorapatite elongated particles growth in gelatin matrices, this study was prepared by Busch S. *et al*. From these

micrographs, a comparison with the immersed powders in this work can be made through the resemblance of the microstructures present [135].

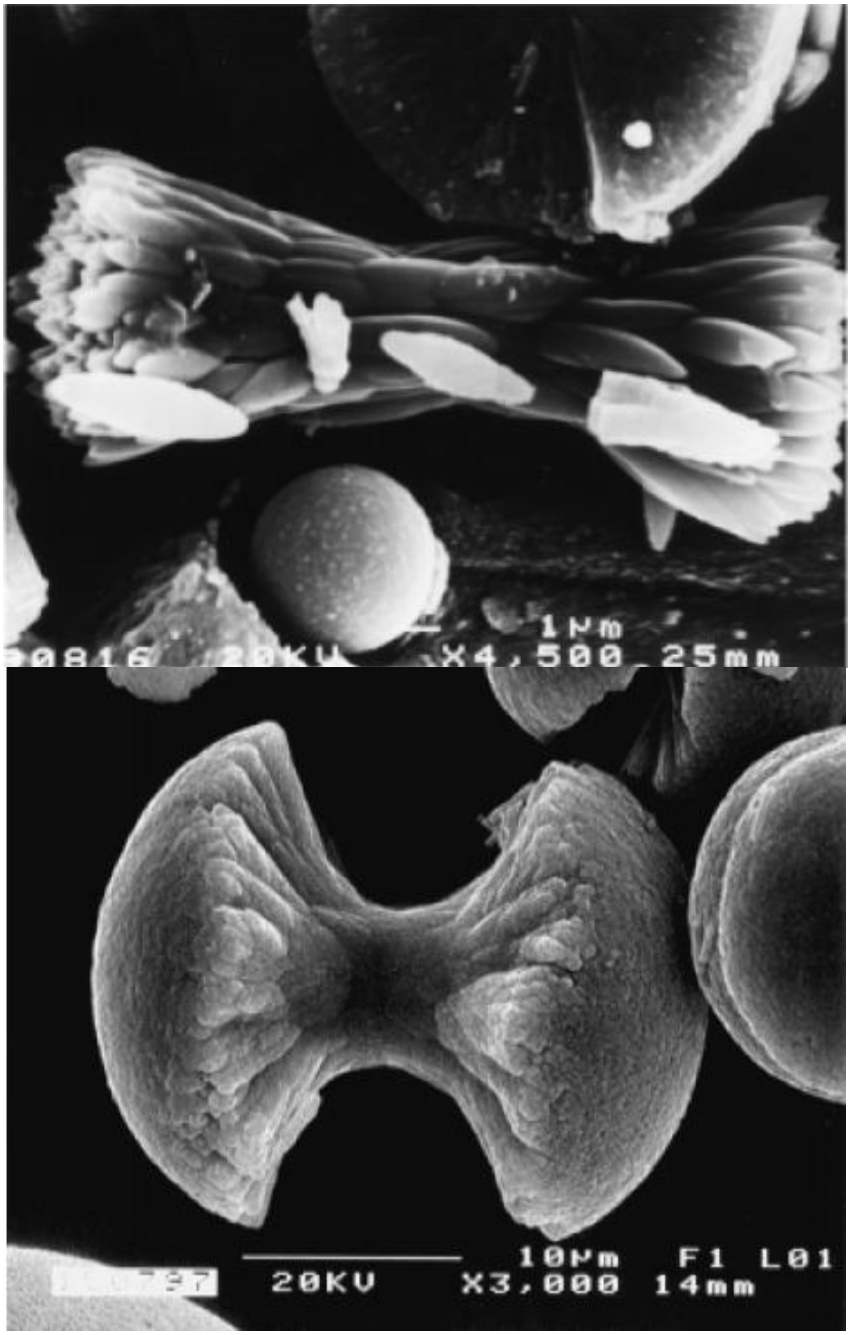

Figure 39 - SEM micrographs of fluorapatite seeds; bottom micrograph is related to a medium-later stage of development of the fluoroapatite seeds [135].

4.3.3. Fourier Transform Infrared Spectroscopy of LNO and LTO powders

In order to fully characterize the lithium niobate and tantalate powders after immersion in SBF, FTIR-ATR spectroscopy was used. The results of measurements are presented in Figure 40 and 41.

Table 8 presents all relevant vibration bands for LNO and LTO immersed in SBF.

Table 8 - Bonds present in the LNO and LTO: vibration frequency and mode of vibration associated [67, 71, 75, 92, 102, 138]

Bands (cm^{-1})	Interpretation
3500-3435	OH bending
2360	OH stretching
2340	Ta=O stretching
1730-1725	C=O stretching
1630-1640	H_2O
1430-1490	CO_3^{2-}
960, 1035-1040	P-O stretching
590 to 870	TaO_6
670-680	Nb=O stretching
620-600, 592-590, 581-580, 574-573, 568	P-O bending

The spectral regions where the most important characteristic bands arise for lithium niobate are 670-681 cm^{-1} that is attributed to NB=O stretching, 960 and 1040 cm^{-1} that was attributed to P-O stretching vibrations, 2360 cm^{-1} attributed to OH stretching, also 3500 cm^{-1} attributed to OH bending and small peaks at 1725-1740 cm^{-1} that probably come from the C=O stretching.

When analyzing the spectra of the FTIRM-ATR from the LNO powders immersed in SBF for 21 days, the presence of peaks at 1040 and 960 cm^{-1},

assigned to P-O vibrations in the PO_4^{3-} group, confirms the formation of calcium phosphate [127].

The absorption band at 671, 679, 681 cm^{-1} is attributed to Nb-O vibration in the crystalline state LNO [67]. The samples also show the absorption bands at 1627, 1630, 1655, 3480 and 3501 cm^{-1}, these bands are attributed to to OH vibration.

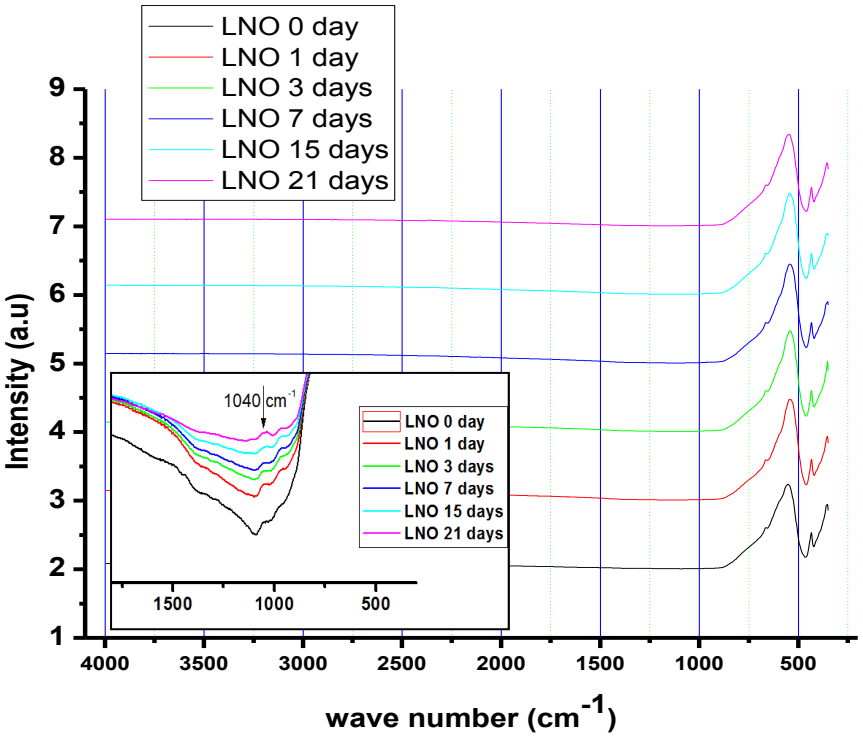

Figure 40 - FTIR-ATR spectra of LNO powders in 0 days immersion and after immersion in SBF for 1, 3, 7, 15 and 21 days.

Observing the plotted graph of LTO immersed in SBF for 21days, FTIR-ATR in Figure 41, an important spectral region appears as TaO_6 band corresponding to the major peaks from 590 to 870 cm^{-1}. One band corresponding to P-O bondings was found at 1040 cm^{-1} suggesting the presence of phosphates in this sample and confirming the previous analysis. Also, for the non-immersed powder, bands at 1430-1490 cm^{-1} assigned to CO_3^{2-} were detected.

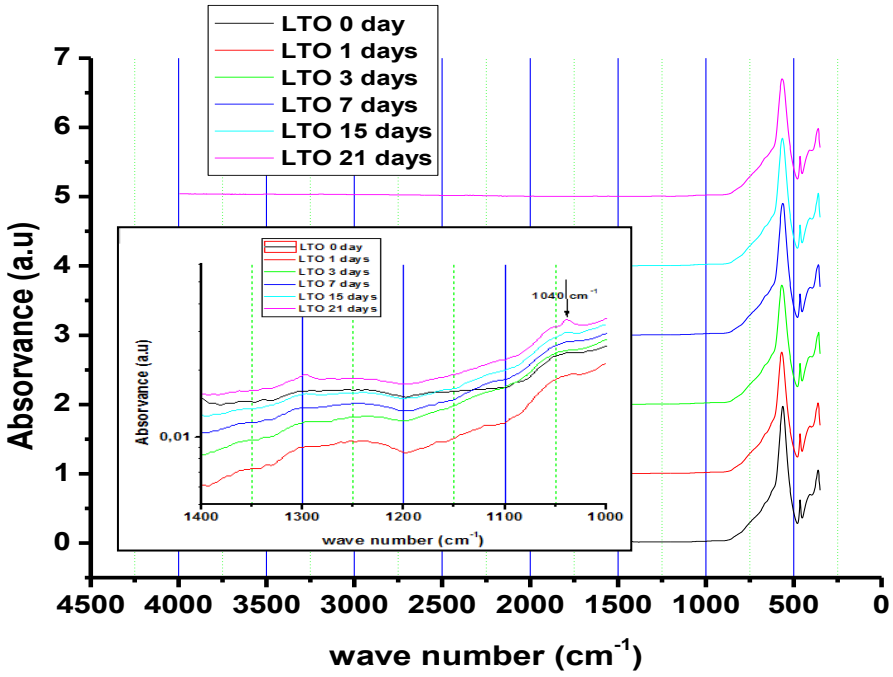

Figure 41 - FTIR spectra of LTO powders before and after immersion in SBF for 1, 3, 7, 15 and 21 days.

4.3.4. Inductively coupled plasma results

In order to investigate the ionic concentration changes of Ca, P and also Li, Nb and Ta in the SBF and predict the ionic exchanges that might have occurred to form the apatite on the surface of the powders, ICPS tests were conducted to SBF solutions after removing the immersed powders.

4.3.4.1. SBF solutions from the LNO powders

As shown in Figure 42, there is a decrease of Ca and P ionic concentration and it occurs mainly after the 7th day of soaking, indicating consumption from the SBF for the growth of Ca-P nuclei that lead to the formation of the calcium phosphate

agglomerates on the surface of the powder, thus confirming the in vitro bioactivity of these materials, believed to be an indication of in vivo bioactivity.

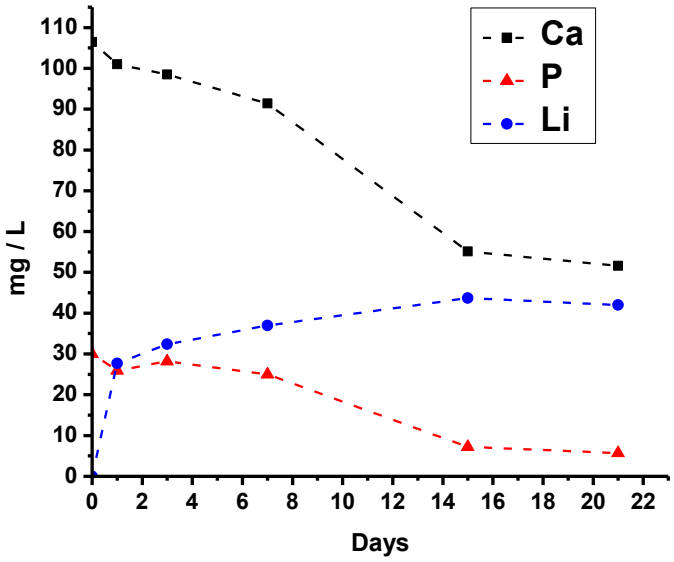

Figure 42 - ICP curve for Ca, P and Li concentration in the SBF that was in contact with the lithium niobate powders from 0 days to 21 days.

Also, from the analysis of Fig. 42, it is observed that the lithium concentration in SBF increases rapidly from 0 to 28 mg/L in one day after immersion of the powder, then this rapid increase is reduced, but still existing from 1 day to 21 days. This increase in Li concentration is attributet to the $LiNbO_3$ dissolution and consequent lithium loss to the liquid.

This means that in an *in vivo* situation, the lithium ion concentration in the biological medium will rapidly increase in just one day after contact which brings up another question: Is Lithium harmful for the human body?

Aral H. et al. reported in 2008 in *"Toxicity of lithium to humans and the environment"*, that "lithium is not expected to bioaccumulate and its human and environmental toxicity are low" [136].

Still, according to Viguera A. et al. lithium is the 27th most abundant element in nature and it is actually used in significant doses (≤10 mg/L in serum) for treatment

of bipolar disorder patients, it is also used for treatment of other mental problems, thus lithium prescription is not recommended for pregnant or lactating women.

It is reported in literature that at 10 mg/L of blood, a human being is midly lithium poisoned, at 15 mg/L they experience confusion and speech impairment, and at 20 mg/L there is a risk of death [137]. In the present work ionic Li concentrations as high as 40 mg/l can be achieved, which corresponds to values that seriously compromise the use of LNO in clinical practice.

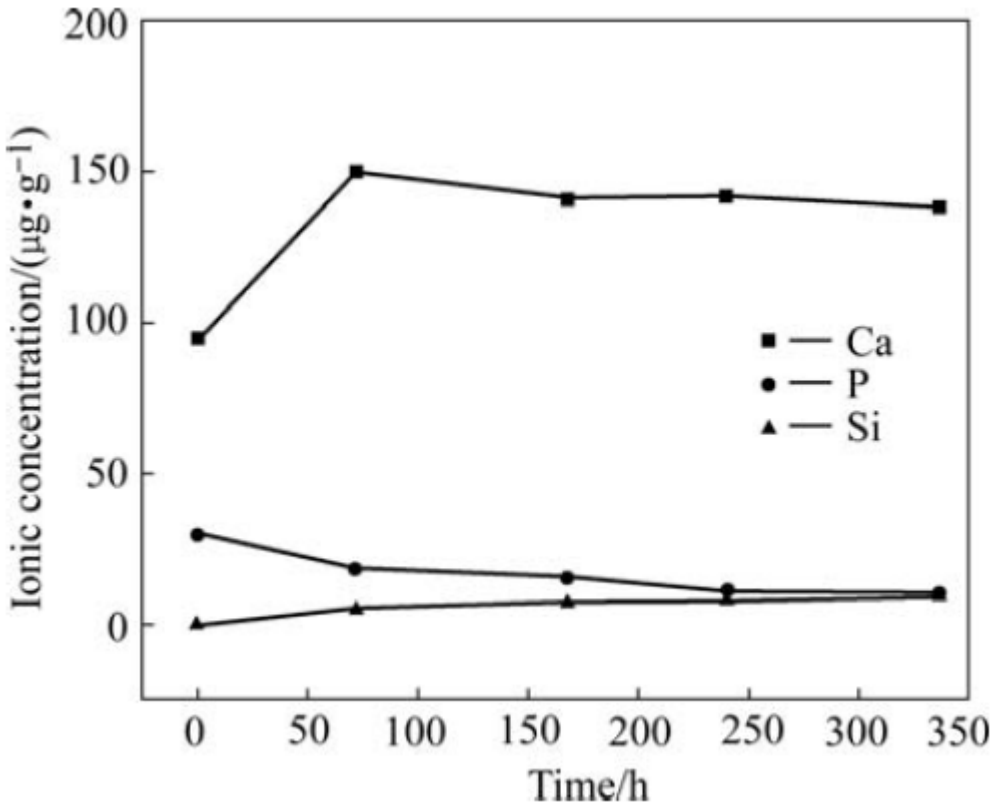

Figure 43 - Variation of Ca, P, and Si ionic concentration on SBF after PLLA/bioactive glass immersion [134].

In Figure 43, there is a representation of an ICP experiment realized by Zhou *et al*. with PLLA immersed in SBF for 350h. From this we can have a notion of calcium, phosphorous and silicium ionic concentration changes in the SBF throughout time for a bioglass composite [134]. A similar approach was realized in this experiment with lithium niobate and tantalite and the results are different. In

the case of PLLA/bioactive glass, there's a steady decrease in the concentration of P, this was due to the fact that the amount of P released from the bioglass wasn't compensating its consumption caused by apatite deposition. In the case of Ca^{2+} there was a higher release from the bioglass in the first 75 hours comparing with the consumption of this ion from the SBF [134].

4.3.4.2. Simulated Body Fluid solutions from the Lithium Tantalate powders

The results from ICP measurements in Figure 44, have shown that the decrease of Ca and P start on day 1, then stabilizes until day 3 and then they are rapidly consumed from the serum until the 15th day soaking. From then on the rate of consumption is decreased until the end of the experiment (21 days). This indicates consumption from the SBF for the growth of the Ca-P nuclei that lead to the formation of the apatite agglomerates on the surface of the LTO powder, confirming the previous SEM / EDS and FTIR results. , The observed behavior suggests *in vitro* bioactivity of these materials, believed to be an indication of their *in vivo* bioactivity.

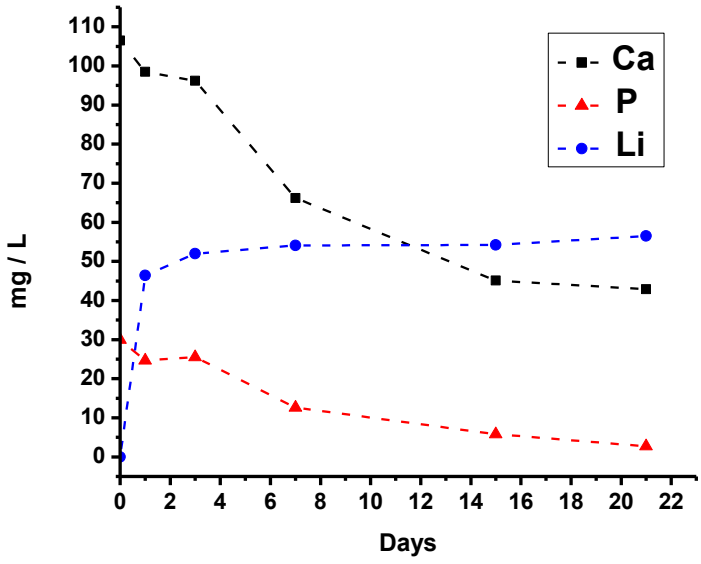

Figure 44 - ICP curve for Li concentration in the SBF that was in contact with the lithium tantalate powders from 0 days to 21 days.

From the analysis of the graph, it is also observed that the lithium ionic concentration in SBF increases rapidly from 0 to 46,4 mg/L one day after immersion of the powder, then this rapid increase is reduced, until 15 days and from 15 to 21 days there is a slight decrease of the slope. The reason why this happens should be very similar to the one reported for the LNO experiments; LTO powder dissolves and lithium is lost to the liquid environment.

Also in the case of LTO the concentration of Li in solution can reach values much higher than the tolerated by the human body. Therefore these findings indicate that although exhibiting interesting properties for application in bone regeneration strategies (namely their potential bioactivity) the use of these materials without additional improvement is associated to a risk for the health of the patients.

Aiming to overcome this drawback a number of solutions can be tested and discussed from the point of view of materials engineering. A way to reduce the excessive Li leaching could be for example (1) the use of higher particle size powders in order to decrease the specific surface area or (2) the realization of a first incubation of the samples (1 day as suggested by Figs 44 and 45 would be enough) in order to promote a first Li lixiviation and a subsequent dissolution within acceptable levels. Another possibility could be the decrease of Li content in the original composition. However this approach may lead to additional constrains.and another question arises: What happens to the ferroelectric properties of both lithium tantalate and lithium niobate, if the stoichiometry of the material is changed?

5. CONCLUDING REMARKS

The deployment of polarized piezoelectric materials has shown the accelerate bone growth. Therefore, in this work, we proposed to study the bioactivity of selected ferroelectric ceramics, specifically Lithium Niobate and Lithium Tantalate, in order to predict possible future applications in medicine for these ferroelectrics if proven bioactive and non-cytotoxic.

Monophasic LiNbO3 and LiTaO3 powders were successfully synthesised in the laboratory at 800°C/5h and no secondary phases were found within the XRD limits.

Our results demonstrate for the first time that lithium niobate and lithium tantalite powders exhibited the formation of inorganic calcium-phosphate agglomerates after immersion in SBF for a certain period. In spite of the absence of XRD indication, may be due to the low crystallinity of the phosphate phases, SEM, FTIR and ICPS analysis provide clear evidences for the formation of calcium phosphates on the surface of LNO and LTO powders. The morphology of these elongated particles was of the typical cauliflower like shape, suggesting the formation of apatite-like precipitates and indicating the probable bioactive behavior of these ferroelectric particles in vivo. The phosphate formation was further confirmed and their stoichiometry quantified by the analysis of the Ca/P ratios; for both LNO and LTO powders the Ca/P ratio of the formed apatite type crystals was 1,65 and 0,68 at 21 days of immersion in SBF. The ICP results showed that Ca and P elements have been consumed from the physiological liquid, and deposited as apatite-like structures on the ceramic powder surface; this behavior is the basis for the formation of calcium-phosphate structures at the interface between a bioactive material and the adjacent living tissue. Also important to note is that during the immersion in SBF there is a significant release of Li from the powder material to the surrounding media, what might be of concern.

These are the first indication of bioactivity of LNO and LTO materials and further studies are required.

5.1. Future recommendations

In order to validate the results obtained in this thesis it is suggested to:

- conduct more experiments with increased soaking times in SBF;
- conduct analysis of the crystallinity of the formed phosphates;
- assess the toxicity of Li, Ta and Nd;
    - increase mean particle size of the boh ceramics;
    - pre-lixiviation of Li on the first days of immersion.
    - decrease Li content in the powders.
- establish the relations between the electrical properties and LNO and LTO stoichiometry;
- to study the influence of electric polarization on acceleration and deceleration of bonelike crystal apatite growth on lithium niobate and lithium tantalate may be an important topic.

6. REFERENCES

1 - Martonosi A. Animal electricity. Ca^{2+} and muscle contraction. A brief history of muscle research. *Acta Biochim Pol* 2000;47: 493-516

2 - (April 2012) *Luigi Galvani*. Available: http://pt.wikipedia.org/wiki/Luigi_Galvani

3 - Burr S., Northrop F. Evidence for the existence of an electrodynamic field in living organisms. *Proc Natl Acad Sci USA* 1939; 25:284-288

4 - Levin M. Bioelectromagnetics in morphogenesis. *Bioelectromagnetics* 2003;24:295-315

5 - Burr H., Lane C., Electrical characteristics of living systems. *Yale J Biol Med* 1935:32-35

6 - Chao P., Roy R., Mauck R., Liu W., Valhmu W., Hung C. Chondrocyte translocation response to direct current electric fields. *J Biomech Eng* 2000;122:261-267

7 - Robinson K. The responses of cells to electrical fields: A review. *J Cell Biol* 1985;191:2023-2027

8 - (June 2012) *Cell Membrane*. Available: http://www.millerandlevine.com/chapter/35/898-899-rewrite.html

9 - Borgens R., Vanable J., Jaffe L. Bioelectricity and regeneration: Large currents leave the stumps of regenerating newt limbs. *Proc Natl Acad Sci USA* 1977;74:4528-4532.

10 - Mycielska M., Djamgoz M. Cellular mechanisms of direct current electric field effects: Galvanotaxis and metastatic disease. *J Cell Sci* 2004;117:1631-1639

11 - Ferrier J., Ross S., Kanehisa J., Aubin J. Osteoclasts and osteoblasts migrate in opposite directions in response to a constant electrical field. *J Cell Physiol* 1986;129:283-288

12 - Ross S. Morphological responses of cells to exogenous ionic currents. *Annu Int Conf IEEE Eng Med Biol* 1990:12;1570-1571

13 - (October 2012) - *Newts Regeneration*. Available: http://news.softpedia.com/newsImage/The-Molecule-of-Limb-Regeneration-Discovered-2.jpg/

14 - Haddad J. Obolensky A. Shinnick P. The biologic effects and the therapeutic mechanism of action of electric and electromagnetic field stimulation on bone and cartilage: New findings and a review of earlier work. *J Altern Complement Med* 2007;13:485-490.

15 - Reilly D., Burstein A. The chemical properties of cortical bone. *J Bone Joint Surg Am* 1974;56:1001-1022

16 - Rodan G. Introduction to bone biology. *Bone* 1992; 13:S3-S6

17 - Sela J., Gross U., Kohavi D., Shani J., Dean D., Boyan B., Schwartz Z. Primary mineralization at the surfaces of implants. *Crit Rev Oral Biol Med* 2000;11:423-436.

18 - Behari J. Elements of Bone Biophysics Biophysical Bone Behaviour: Principles and Applications. *Wiley*; 2009. p1-52

19 - Ross F., Cristiano A., Nothing but skin and bone. *J Clin Invest* 2006;116:1140-1149.

20 - Currey J. Changes in the impact energy absorption of bone with age. *J Biomech* 1979;12:459-469

21 - Rosenbaum T., Bloebaum R., Ashrafi S., Lester D. Ambulatory activities maintain cortical bone after total hip anthroplasty. *Clin Orthop Relat Res* 2006;450:129-137.

22 - Frost H. Mechanical determinants of bone modelling. *Metab Bone Dis Relat Res* 2006;86:1000-1006

23 - Lane J., Vogorita V. Osteoporosis. *J Bone Joint Surg Am* 1983;65:274-278.

24 - Shea K., Ford T., Bloebaum R., King H. A comparison of microarchitectural bone adaptations, the concave and convex thoracic spinal facets in idiopathic scoliosis. *J Bone Joint Surg Am* 2004;86:1000-1006.

25 - Skedros J., Baucom S. Mathematical analysis of trabecular 'trajectories' in apparent trajectorial structures: The unfortunate historical emphasis on the human proximal femur. *J Theor Biol* 2007;244:15-45.

26 - Currey J. The mechanical properties of bone. A review. *Clin Orthop* 1970;73:210-232.

27 - Singh S., Saha S. Electrical properties of bone. A review. *Clin Orthop Relat Res* 1984;186:249-271.

28 - Chakkalakal D., Johnson M. Electrical properties of compact bone. *Clin Orthop Relat Res* 1981;161:133-145

29 - Yasuda I. Electrical callus and callus formation by electret. *Clin Orthop Relat Res* 1977;124:2-4

30 - Brighton C. Bioelectrical effects on bone and cartilage. *Clin Orthop relat Res* 1977;124:2-4.

31 - Yasuda I. The classic fundamental aspects of fracture treatment. *Clin Orthop Relat res* 1977;124:5-8.

32 - Friendenberg Z., Brighton C. Bioelectric potentials in bone. *J Bone Joint Surj Am* 1966;48:915-923

33 - Victoria G., Petrisor., Drew B., Dick D. Bone stimulation for fracture healing: What's all the fuss? *Indian J Orthop* 2009;43:117-120.

34 - Spadaro J. Mechanical and electrical interactions in bone remodeling. *Bioelectromagnetics* 1997;18:193-202

35 - Rubinacci A., Tessari L. A correlation analysis between bone formation rate and bioelectric potentials in rabbit tibia. *Calcif Tissue Int* 1983;35:728-731.

36 - Fukada E., Yasuda I., On the piezoelectric effect of bone. *J. Phys Soc Jpn* 1857;12:1158-1162.

37 - Baxter F., Bowen C., Turner I., Dent A. Electrically Active Bioceramics: A Review of Interfacial Responses. *Ann Biomed Eng* 2010;38:2079-2092.

38 - Fukada E., Yasuda I., Piezoelectric effects in collagen. *Jpn J Appl Phys* 1964;3:117-121.

39 - (October 2012) *Eiichi Fukada*. Available: http://www.coe.ou.edu/isb/awardees/1995.htm

40 - Lavine L., Grodzinsky A. Electrical stimulation of repair of bone. *J Bone Joint Surg Am* 1987;69:626-630.

41 - Bassett C., Becker R. Generation of electric potentials by bone in response to mechanical stress. *Science* 1962;137:1063-1064.

42 - Rho J., Spearing L., Zioupos P. Mechanical properties and the hierarchical structure of bone. *Medical Engineering & Physics*, Volume 20, 1998;2:92-102

43 - Currey J. Comparative mechanical properties and histology of bone. *Am Zool* 1984;24:5-12.

44 - Buckwalter J., Glimcher M., Cooper R., Recker R. Bone biology. *J Bone Joint Surg Am* 1995;77:1276-1289.

45 - Marino A.Electrical stimulation in orthopaedics: Past, present and future. *J Bioelectricity* 1984;3:235-244.

46 - Nyman J., Roy A., Shen X., Acuna R., Tyler J., Wang X. The influence of water removal on strength and toughness of cortical bone. *J Biomech* 2006;39:931-938.

47 - Anderson J., Eriksson C. Piezoelectric properties of dry and wet bone. *Nature* 1970;227:491-492.

48 - Lente F. Cases of un-united fracture treated by electricity. *N Y J Med* 1850;5:317-319.

49 - Hartshorne E. On the causes of treatment of pseudoarthrosis and especially that form of it sometimes called supernumerary joint. *Am J Med Sci* 1841;1:121-156.

50 - Mercola J., Kirsch D. The basis of microcurrent electrical therapy in conventional medical practice. *J Adv Med* 1995;8107-120.

51 - Hastings G., Mahmud F. The electromechanical properties of fluid-filled bone: a new dimension. *J Mater Sci Mater Med* 1991;2:118-124.

52 - (November 2012) *Collagen Orientation*. Available: http://ittcs.wordpress.com/2010/06/01/anatomy-and-physiology-the-intervertebral-discs/

53 - Cowin S., Moss M. Mechanosensory mechanisms in bone. In: Bone Mechanics Handbook, edited by Cowin S. Boca Raton:*CRC Press* 2001.

54 - Frost H.Update of bone physiology and Wolff's Law for clinicians. *Angle Orthod* 2004;74:3-15.

55 - Cowin S., Weinbaum S., Zeng Y. A case for bone canaliculi as the anatomical site of strain generated potentials. *J Biomech* 1995;28:1281-1297.

56 - Jaymes E. Ferroelectricity. *Princeton Univ Press* 1953;1:18-30

57 - Littlewood P. Physics of ferroelectrics. *PB Littlewood*, 2002

58 - Vilarinho P. Functional Materials: Properties, Processing and Applications, in Scanning Probe Microscopy: Characterization, Nanofabrication and Device Application of Functional Materials, 3 -33., 2005, edited by P. M. Vilarinho, Yossi Rosenwaks and Angus Kingon, *Kluwer Academic Publishers*.

59 - Sikalidis C. Electric and Magnetic Ceramics, Bioceramics, Ceramics and Environment - *Advances In Ceramics*, 2011.

60 - Haertling G. Ferroelectric Ceramics: History and Technology – *Journal of American Ceramics Society*, 82 [4] 797–818, 1999.

61 - Cheng J., Wang B., Du S. A statistical model for predicting efective electro-elastic properties of polycrystalline ferroelectric ceramics with aligned defects. *International Journal of Solids and Structures*. 2000;37:4763-4781.

62 - (June 2012) *Perovskite*. Available: http://mrc.iisc.ernet.in/Images/Research_Areas/Original/Image1_Perovskite.jpg

63 - Navale S., Gaikwad A., Ravi V. A coprecipitation technique to prepare $LiTaO_3$ powders. *Materials Letteres* 2006;60:1047-1048

64 - Bowen H. *Mater Sci. Eng*. 1980;44:1

65 - Jean J. Chemical preparation of spherical lithium tantalate powder. 1990;25:2267-2273

66 - Liu M., Xue D. An efficient approach for the direct synthesis of lithium niobate powders. *Solid State Ionics* 2006;177:275-280

67 - An C., Tang K., Wang C., Shen G., Jin Y., Qian Y. *Mater Res Bull*. 2002;37:1791.

68 - Dey D., Kakihana M. *J Ceram Soc Jpn*. 2004;112:368.

69 - Camargo E., Kakihana *M. Chem Mater*. 2001;13:1905.

70 - Niederberger M., Pinna N., Polleux J., *Antonietti. Chem Int Ed*. 2004;43:2270.

71 - Zhang X., Xue D., Liu M., Ratajczak H. Xu D. Microscopically structural studies of lithium niobate powders. *J Molecul Struc*. 2005;754:25-30.

72 - Kalinnikov V., Gromov O., Kunshima G., Kuzmin A., Lokshin E., Ivanenko V. *Inorg Mater*. 2004;40:411.

73 - Svaasand L., Eriksrud M., Nakken G., Grande A.: *J. Cryst. Growth* 1974;22:230.

74 - Camargo E., Kakihana *M. Solid State Ionics*. 2002;151:413.

75 - Liu M., Xue D., Zhang S., Zhu H., Wang J., Kitamura K. Chemical synthesis of stoichiometric lithium niobate powders. *Mater Letters*. 2005;59:1095-1097.

Imagem 76 - Xue D., Kitamura K., Wang J. Atomic packing and octahedral linking model of lithium niobate single crystals. *Optical Materials* 2003;23:399–402

77 - Kuo C., Chen G., Chang Y., Fu J., Chang Y., Hwang W. Thermal behavior of the nonstoichiometric lithium niobate powders synthesized via a combustion method. *Ceramics International* 2012;38:3729–3733

78 - Muthurajan H., Kumar H., Natarajan N., Ravi V. A novel technique to prepare $LiTaO_3$ at low temperature. *Cer Int*. 2008;34:669-670.

79 - Zhang Y., Jia D., Zhou Y., Meng Q., Liu Y., Ke H. Sintering mechanism and dielectric properties of LiTaO3 matrix composites with the addition of Al_2O_3 particles. *Cer Int*. 2009;35:3474-3478.

80 - Brinker C., Clark D., Ulrich D. *Better ceramics through Chemistry*, Vol 1. 1984.

81 - Moulson A., Herbert J. Electroceramics: Materials, properties and applications. *Chapman and Hall*, London, 1990.

82 - Ravez J., Joo G., Bonnet J. Ferroelectric properties of $Li_{0.8}Mg_{0.2}(-Ta_{0.8}Ti_{0.2})O_3$ ceramics, *Ferroelectrics* 1998;81:305-308.

83 - Sinclair D., West A. Electrical properties of $LiTaO_3$ single crystal, *Physical Review B.* 1989;39:13486-92

84 - Gonhzalez A., Simoes A., Zaghete M., Varela J. Mater Charact. 2003;50:233.

85 - Deis T., Phule P. Mater Res Bull. 1993;28:167.

86 - Ye Z., Muhll V., Ravez J. Mater Sci Eng, Solid-state Mater Adv Technol. 1989;5:47

87 - Kolb E., Laudise R. J Cryst Growth. 1976;33:145.

88 - Skólska I., Kuck S. Optical characterization of Cr^{3+} doped $LiTaO_3$ crystals relevant for laser application. *Spectrochim Acta A*. 1998;54:1695-1700

89 - Inoue Y., Kato Y. *Chem Soc, Faraday Trans*. 1992;88:449-454.

90 - Hosaka N., Yuhara A., Yamada J., Kobayashi T. *J Appl Phys.* 1990;29:154-156

91 - Salavcova L., Spirkova J., Ondracek F., Mackova A., Vacik J., Kreissig U. et al. Study of anomalous behaviour of $LiTaO_3$ during the annealed proton exchange process of optical wveguide's formation - comparison with $LiNbO_3$. *Opt Mater*. 2007;29-913-918.

92 - Zielinska B., Mijowska E., Kalenczuk R. Synthesis, characterization and photocatalytic properties of lithium tantalate. *Mater Charac*. 2012;68:71-76.

93 - Muthurajan H., Kumar H., Natarajan N., Ravi V. *Ceram Int*. 2008;34:669-670.

94 - Bamba N., Yakouchi T., Takaoka J., Elouadi B., Fukami T. Effects of CaTaO3 on electrical properties in $LiTaO_3$ ceramics. *Ferroelectrics.* 2004;304:135-138.

95 - Rocchiccioli-Deltcheff M. Spectrochim. *Acta 29A*. 1972;93.

96 - Hultgren R., Orr R., Anderson P., Kelly P. Selected values of thermodynamic properties of metals and alloys, *Wiley, New York*. 1963;pp. 153-157.

97 - Yan S., Wang Z., Li Z., Zou Z. Photocatalytic activities for water splitting of La-doped-NaTaO3 fabricated by microwave synthesis. Solid State ionics. 2009;180:1539-1542.

98 - Phule P., Deis T., Dindiger D. *J Mater Res*. 1991;6:1567

99 - Castaings N., Duboudin F., Ravez J., Hagenmuller P. *Mater Res Bull*. 1987;22:261.

100 - Lauf R. Bond N. *Amer Ceram Soc Bull*. 1984;63:278.

101 - Muthurajan H., Kumar H., Natarajan N., Ravi V. *Ceram Int*. 2008;34:669-210.

102 - Zheng F., Liu H., Yao S., Yan T., Wang J. Hydrothermal and wet-chemical synthesis of pure $LITaO_3$ powders by using commercial tantalum hydroxide as starting material*. Journal of Alloys and Compounds*. 2009;477:688-691.

103 - Bajpai P., Billote W. Ceramic Biomaterials. In: Bronzino JD. The Biomedical Engineering Handbook, *Boca Raton:CRC Press*. 1995:552-580.

104 - Hench L. Bioactive Glasses Mechanisms of Bioactive Bonding. *Web*:1-25.

105 - Hench L., Bioceramics. *J. Am Ceram Soc.* 1998;81:1705-1728.

106 - Hench L. Ceramics, Glasses and Glass-Ceramics. *Biomaterials Science - An Introduction to Materials in Medicine*. 1996:73-84.

107 - Hench L. Bioceramics: From Concept to Clinic. *J Am Ceram Soc*. 1991;74:1487-1510

108 - Sorrell C. Silicon Nitride and Related Nitrogen Ceramics: I. Phase Equilibria and Properties of Reaction Bonded and Hot Pressed M-Si-O-N Systems. *J Aust Ceram Soc*. 1982;18:22-23.

109 - Ziegler G., Heinrich J., Wotting G. Review: Relationships between processing microstructure and properties of dense and reaction-bonded silicon nitride. *J Mater Sci.* 1987;22:3041-3086

110 - Hench L., Wilson J. Bioactive Glasses and Glass-ceramics: A 25-year Retrospective. *Bioceramics: Materials and Applications*. 1995;48:11-12.

111 - Black J. Biological Performance of Materials: fundamentals of biocompatibility. *New York: Marcel Dekker, Inc*. 1992:286-299.

112 - Wilson J., Yli-Urpo A., Risto-Pekka H. Bioactive glasses: clinical applications. An introduction to bioceramics. Singapore: *World Scientific*. 1993:63-74.

113 - Kitsugi T., Nakamura T., Yamamuro T., Kokubo T., Shibuya T., Takagi M. SEM-EPMA observation of three types of apatite containing glass-ceramics implanted in bone: the variance of a Ca-P rich layer. *J Biomed Mater Res.* 1987;21:1255-1271.

114 - Kokubo T. Ito S., Huang Z., Hayashi T., Sakka S., Kitsugi T., Yamamuro T. Ca, P-rich layer formed oh high-strength bioactive glass-ceramic A-W. *J Biomed Mater Res.* 1990;24:331-343.

115 - Kokubo T. Surface chemistry of bioactive glass-ceramics. *J Non-Cryst Solids*. 1990;120:138-151.

116 - Ohtsuki C., Kushitani H., Kokubo H., Kotani S., yamamuro T. Apatite formation on the surface of Ceravital-type glass-ceramic in the body. *J Biomed Mater Res.* 1991;25;1363-1370.

117 - Kitsugi T., Yamamuro T, Kokubo T., Analysis of A-W glass-ceramic surface by micro-beam X-ray diffraction. *J Biomed Mater Res.* 1990;24:259-273.

118 - Loty C., Sautier J., Boulekbache H., Kokubo T., Kim H., Forest N. In vitro bone formation on a bonelike apatite layer prepared by a biomimetic process on a bioactive glass-ceramic. *J Biomed Mater Res* 2000;49:423-34.

119 - Neuman W., Neuman W. The chemical dynamics of bone mineral. Chicago: *University of Chicago Press, IL*, 1958.

120 - Gamble J., Chemical anatomy, physiological and pathology of extracellular fluid. Cambridge, *MA: Harvard University Press*. 1967.

121 - Kokubo T., Kushitani H., Sakka S. Solution able to reproduce in vivo surfacestructure changes in bioactive glass-ceramic A-W. *J Miomed Mater Res* 1990;24:721-734.

122 - Kokubo T. Kushtani H., Ebisawa Y., Kitsugi T., Kotani S., Ohura K., Yamamuro T. Apatite formation ob bioactive ceramics in body environment. In: OOnishi H. Aoki H., Sawai K. *Bioceramics*, vol1. Tokyo: Ishiyaku Euro America, 1989. p. 157-162.

123 - Ebisawa Y., Kokubo T., Ohura K., Yamamuro T. Bioactivity of CaO-SiO_2 glasses: in vitro evaluation. *J Mater Sci Mater Med* 1993;1:239-244.

124 - Filguerias M., Torre G., Hench L. Solution effects on the surface reaction of a bioactive glass*. J Biomed Mater Res.* 1993;27:445-453.

125 - Ohtsuki C., Aoki Y., Kokubo T., bando Y., Neo M., Nakamura T. Transmission electron microscope observation of glass-ceramic A-W and apatite layer formed on its surface in a simulated body fluid. *K Ceram Soc Japan*. 1995;103:449-454.

126 - Kokubo T., Takadama H., "How useful is SBF in predicting in vivo bone bioactivity?", *Biomaterials*. 2006;27:2907–2915

127 - Stanciu G., Sandulescu I., Savu B, Stanciu S., Paraskevopoulos K., Chatzistavrou X, Kontonasaki E., Koidis P. Investigation of the Hydroxyapatite Growth on Bioactive Glass Surface - *Journal of Biomedical & Pharmaceutical Engineering* 2007;1:34-39

128 - Landia E., Celottia G., Logroscinob G., Tampieria A. Carbonated hydroxyapatite as bone substitute - *Journal of the European Ceramic Society* 2003;23:2931–2937

129 – Lanza R., Langer R., Vacanti J. Principles of Tissue engineering, 3rd Edition, *Elsevier*, 2007.

130 – The emergence of tissue Engineering as a Research Field, NSF, USA, 2003.

131 – Barroca N., Vilarinho P. M., Daniel-da-Silva A., Wu A., Fernandes M. H., Gruverman A. Protein absorption on piezoelectric poly-L-lactic acid thin films by scanning probe microscopy. *Applied Physics Letters*. 2011;98:133705.

132 - Länge K., Rapp B., Rapp M. Surface acoustic wave biosensors: a review. *Anal Bioanal Chem* 2008;391:1509–1519

133 - Balamurugan A., Balossier G., Kannan S., Michel J., Rebelo A., Ferreira J. Development and in vitro characterization of sol–gel derived $CaO–P_2O_5–SiO_2–ZnO$ bioglass - *Acta Biomaterialia* 2007;3:255–262.

134 - Zhou Z., Jian-ming R, Jian-peng Z., Zhong-cheng Z, Xiong-jun S. Bioactivity of bioresorbable composite based on bioactive glass and poly-L-lactide. *Trans. Nonferrous Met. Soc China* 2007;17:394-399

135 - Busch S., Dolhaine H., DuChesne A., Heinz S. Hochrein O., Laeri F., Podebrad O., Vietze U., Weiland T., Kniep R. Biomimetic Morphogenesis of Fluorapatite-Gelatin Composites: Fractal Growth, the Question of Intrinsic Electric Fields, Core/Shell Assemblies, Hollow Spheres and Reorganization of Denatured Collagen. Eur. *J. Inorg. Chem.* 1999;1643-1653

136 - Aral H., Sadus A. Toxicity of lithium to humans and the environment - A literature review. *Ecotoxicology and Environmental Safety*. 2008;70:349-356.

137 - Viguera A., Cohen L., Baldessarini R., Nonacs R. Managing bipolar disorder during pregnancy: weighting the risks and benfits*. Can J Psychiatry* 2002;47:426-436.

138 - Barroca N., Daniel-da-Silva A., Vilarinho P.M., Fernandes M.H.V. Tailoring the morphology of high molecular weight PLLA scaffolds through bioglass addition. *Acta Biomaterialia* 2010;6:3611-3620

139 - Gonnard P. Guide on the best piezoelectric properties of lead-free single crystals. *POLECER Thematic Network Workpackage 9*. 2004